Injection Locked Oscillator for Radiometer

Sushan Khadka

School of Electrical Engineering

Thesis submitted for examination for the degree of Master of Science in Technology.
Espoo 15.09.2019

Supervisor

Prof. Jussi Ryynänen

Advisor

D.Sc. Kari Stadius

Aalto University
School of Electrical
Engineering

Aalto University
School of Electrical
Engineering

Aalto University, P.O. BOX 11000, 00076 AALTO
www.aalto.fi
Abstract of the master's thesis

Author Sushan Khadka

Title Injection Locked Oscillator for Radiometer

Degree programme School of Electrical Engineering

Major Micro- and Nanoelctronic Circuit Design **Code of major** ELEC3036

Supervisor Prof. Jussi Ryynänen

Advisor D.Sc. Kari Stadius

Date 15.09.2019 **Number of pages** 46 **Language** English

Abstract

The main goal of this project was to design an injection locked oscillator (ILO) with free-running frequency of 70 GHz, and with locking capability to the third and the fifth harmonics of the reference signal upon injection. The circuit was realized using the silicon-germanium (SiGe) bipolar-complementary metal-oxide-semiconductor (BiCMOS) technology and the locking condition were verified after simulating the resistor-capacitor (RC) extracted netlist of the layout. The cadence virtuoso toolkit was used for the design process and the simulation purpose. The locking phenomenon, quasi-lock and fast-beat mode, lock range upon different injection power and phase noise characteristics of the ILO upon subharmonic injection were studied.

The ILO was implemented using the direct (parallel) injection topology. The designed ILO circuit consists of two main components; conventional cross-coupled oscillator with oscillation frequency of 71 GHz and harmonic generator that injects the harmonics of the reference signal into the oscillator. The nonlinearities of the transistor were studied under different biasing conditions and the optimal bias point of 0.83 V was chosen that provided the maximum frequency conversion gain. The power consumed by the core oscillator is 2.64 mW and 3.4 mW by the harmonic generator under the supply voltage of 1.2 V, making the total power consumption of 6.04 mW as a whole by the ILO.

The ILO achieved the locking range (LR) of 7.9% for the fifth harmonics injection and 1.22% for the third harmonics injection of the reference signal with input injection power of 0 dBm. The oscillator even achieved 0.32% LR for the seventh harmonics injection with the injection power of 0 dBm. The corresponding frequency ranges are 18.9-24.5 GHz, 13.29-14.16 GHz, 9.8-10.03 GHz for the third, fifth and the seventh harmonics injection respectively.

Keywords Injection Locked Oscillator, Subharmonic Injection Locking, Phase Noise, Harmonic Generator, Lock Range

Preface

First and foremost, I would like to express my profound gratitude and sincere thanks to my supervisor Prof. Jussi Ryynänen and advisor Kari Stadius for providing me an opportunity to work on this project. I am specially grateful to my advisor, Kari Stadius, for his guidance and support throughout the entire thesis period.

I am very thankful to the Andreas Hammer, Faizan Ul Haq and Yehia Twafik for their invaluable technical support. Also, deepest thanks to my friend and brother, Subash Puri, who has always inspired me to target for higher goals in life.

Most of all, I would like to remember my parents, Krishna and Manju, everything i have ever achieved in my life belongs to their immense love and support. Finally, my brothers, Nishan and Roshan, I love you guys.

Otaniemi, 29.8.2019

Sushan Khadka

Contents

Symbols and abbreviations

Symbols

Q	Quality Factor
ω	Arbitrary Frequency
ω_0	Oscillation Frequency in Radians per Second
ω_{inj}	Injection Frequency
f_0	Oscillation Frequency in Hertz
$\mathcal{L}_{\Delta\omega}$	Phase Noise
$\Delta\omega$	Offset Frequency From the Main Oscillation Frequency
$H(j\omega)$	Open-Loop Gain
$\beta(j\omega)$	Feedback Transfer Function
P_{DC}	DC Power Consumption
g_m	Small Signal Transconductance
C_π	Base-Emitter Capacitance
C_μ	Base-Collector Capacitance
C_{cs}	Collector-Substrate Capacitance
R_p	Inductor Equivalent Parallel Resistance
R_s	Inductor Effective Series Resistance
I_{tail}	Oscillator Bias Current
$\vec{I}_{tank}$	Tank Current
$\vec{I}_{osc}$	Oscillation Current
$\vec{I}_{inj}$	Injection Current
V_{osc}	Output Voltage Swing of the Oscillator
θ	Phase Difference Between Tank Current and Oscillation Current
ϕ	Angle Between Oscillation Current and Injection Current
φ	Small Random Phase Fluctuations
ω_L	Lock Range

Abbreviations

DC	Direct Current
ILO	Injection Locked Oscillator
LC	Inductor-Capacitor
RC	Resistor-Capacitor
RLC	Resistor-Inductor-Capacitor
LR	Lock Range
FOM	Figure of Merit
RF	Radio Frequency
HBT	Hetrojunction Bipolar Transistor
BJT	Bipolar Junction Transistor
CMOS	Complementary Metal-Oxide-Semiconductor
BiCMOS	Bipolar Complementary Metal-Oxide-Semiconductor
IC	Integrated Circuit
DFT	Discrete Fourier Transform
ADS	Advance Design System
RFIC	Radio Frequency Integrated Circuit
PLL	Phase-Locked Loop
IV	Current-Voltage
EM	Electromagnetic

1 Introduction

Communication systems have been developed rapidly over the past few decades. The requirement of high data rate communication systems with low power and low voltage headroom, occupying the smaller dye area is inevitable. In the recent years, the millimeter-wave (mm-wave) frequency band (30-300 GHz) has got a lot of attention, opening the gateway for high data rate communications, radars, material characterization, security and medical applications. On the other hand, the design of a high performance, low power and low-cost radio frequency (RF) circuit becomes a challenging task for the engineers with the technology scaling. The advanced CMOS and SiGe BiCMOS process has become most preferred technology for designing extremely high-speed RF electronics that offers cost-effective and low power solutions. These process with bipolars offer transient frequency higher than 300 GHz.

The larger number of channels are required with the growing wireless communication systems. The requirement of reference signal with less phase noise becomes very essential in transceivers to avoid signal corruption due to frequency conversion of the undesired channel. The limited performance of active and passive components at high frequencies degrades the spectral purity of the local oscillator signals. The phase noise must be very small so that the negligible amount of corruption is produced. The traditional phase-locked loop (PLL) phase noise increases as the frequency of operation increases, consumes high power and occupies large area. In spite of having high phase noise performance than most of the available oscillators, inductor-capacitor (LC) oscillators also suffer from poor phase noise performance due to low quality factor (Q) of the on-chip inductors. ILO is a suitable candidate for mm-wave frequency applications to overcome these problems as it allows the transformation of low quality signal to the signal of high spectral purity. The oscillator can be locked to the subharmonic frequency of the reference signal with excellent phase noise performance. The resulting output signal of the oscillator follows the phase noise of the injection signal, improving the phase noise performance of the oscillator.

The sole purpose of this project was to design an ILO with free running frequency of 70 GHz. The main core oscillator must be locked by the third and the fifth harmonics of the reference signal which are 23.33 GHz and 14 GHz respectively. The goal of the project was achieved utilizing the direct injection topology with cross-coupled topology as the core oscillator, and the differential harmonic generater that depends upon the nonlinearity of transistor to generate all the harmonics of the reference signal.

Section 2 presents the fundamental principle for oscillation and basic theory on different integrated oscillators. Section 3 describes the theory of injection locking phenomenon, mathematical derivation of locking range (LR) and phase noise characteristics of the ILO. Section 4 presents the ILO design description and its layout implementation. Section 5.3 presents the simulated results of the designed ILO.

2 Oscillator Fundamentals

In electronics, oscillators are nonlinear devices that converts direct-current (DC) signal into alternating-current (AC) signal of desired frequency. Oscillators generate periodic waveforms that could be either sinusoidal, triangular, square or distorted version of all the three. Oscillators are extensively used in various electronic devices such as reference tone in receivers and transmitters, master clocks in computers, frequency synthesizers, wristwatches and so on. They are implemented either as single ended or in differential form depending upon the requirement of the system. However, mostly differential configuration is desired due to its less power consumption, common mode rejection and less phase noise. Besides, many RF applications require reference signal with amplitude stability and high spectral purity [1–3].

2.1 The LC Resonator

LC resonators often called tank circuits are the most commonly used resonators in integrated RF oscillators. The output of a LC resonator has a bandpass response with maximum amplitude at the resonance frequency. It plays an important role in overall performance of an oscillator as it affects the amplitude of oscillation, tuning range and phase noise. With some initial energy given, an ideal LC tank oscillates for eternity. But, in practice, due to ohmic resistance of the capacitor and the inductor, the oscillation decays with certain damping frequency at every instant of time until it completely dies out as shown in Figure 1(c).

High performance capacitors can be easily implemented in integrated circuits (ICs). But, the loss introduced by the semiconducting substrates in silicon technology limits the Q of an inductor; Q is a dimensionless quantity and, is defined as the ratio of the energy stored to the energy lost per cycle within the resonator. In addition, larger inductor demands bigger silicon area which restricts its on chip implementation. Also, the self resonant frequency (SRF) of the integrated inductors limits its frequency of operation. Figure 1(a) and Figure 1(b) shows the model of a lossy LC resonator and its equivalent parallel resistor-capacitor-inductor (RLC) circuit respectively.

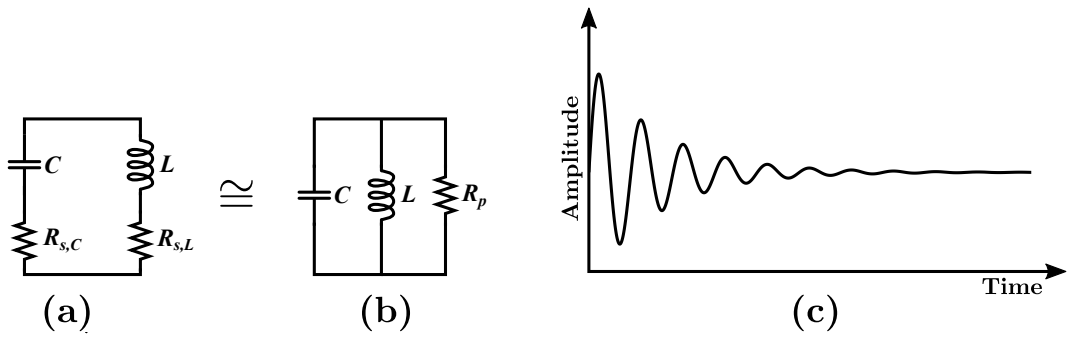

Figure 1: (a) Lossy LC resonator: $R_{s,C}$ and $R_{s,L}$ models the loss of the capacitor and the inductor respectively. (b) Equivalent parallel RLC model. (c) Oscillatory behaviour of a lossy resonator.

The values of the capacitor C and the inductor L determine the oscillation frequency of the resonator, and is given by:

$$\omega_0 = \frac{1}{\sqrt{LC}} \tag{1}$$

where ω_0 is natural frequency of the LC resonator. The effective impedance Z_p of the resonator in parallel configuration is:

$$|Z_p| = \frac{1}{\sqrt{\left(\frac{1}{R_p}\right)^2 + \left(\frac{1}{\omega L} - \omega C\right)^2}} \tag{2}$$

where ω is any arbitrary frequency and R_p is an equivalent parallel resistance of the lossy resonator as depicted in Figure 1(b). Eq. (2) implies that the impedance of the inductor and the capacitor dominates at high frequencies and at low frequencies respectively. At resonance, the inductive and capacitive impedances cancel out, therefore, the impedance is simply the resistance of the network.

$$|Z_p| = R_p \tag{3}$$

Eq. (4) shows the relation of Q with the LC tank. The expression comes in very handy for rough estimation of the Q while designing the RF circuits.

$$Q = R_p \omega_0 L = \omega_0 R_p C = \frac{1}{R_p}\sqrt{\frac{L}{C}} \tag{4}$$

2.2 Basic Principle and Condition for Oscillation

To sustain the oscillation, an active device can be connected in parallel to the tank that injects energy to the tank to compensate the loss introduced by the passive components. The active devices are generally implemented using metal-oxide-semiconductor field-effect transistors (MOSFETs) or bipolar junction transistors (BJTs) with feedback loop that exhibits negative resistance when seen from the resonator [4]. Figure 2 shows the conceptual view of the resonator along with the active circuit. With $|-R_p| \geq R_p$, any noise starts the oscillation whose amplitude grows with time until it reaches steady state [1].

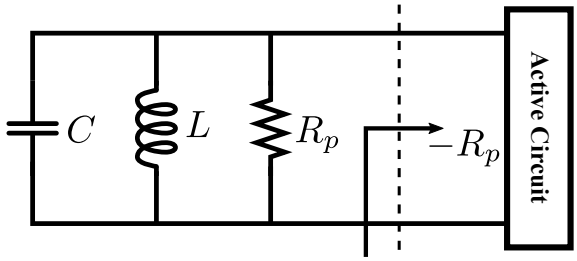

Figure 2: LC tank with active circuit added to cancel the loss.

In 1934, while studying the feedback oscillators, H. G. Barkhausen developed a formula that an oscillator must fulfill to sustain a steady oscillation which are often referred as phase and gain conditions for oscillation . It is a necessary criterion but does not guarantee oscillation at the desired frequency [5].

An oscillator can be modeled as two blocks as shown in Figure 3 that consists of an amplifier and a feedback circuit. Though, the feedback loop configuration is negative feedback in real implementation, at frequency of operation, the feedback becomes positive due to the total phase shift provided by the amplifier and the feedback loop [6].

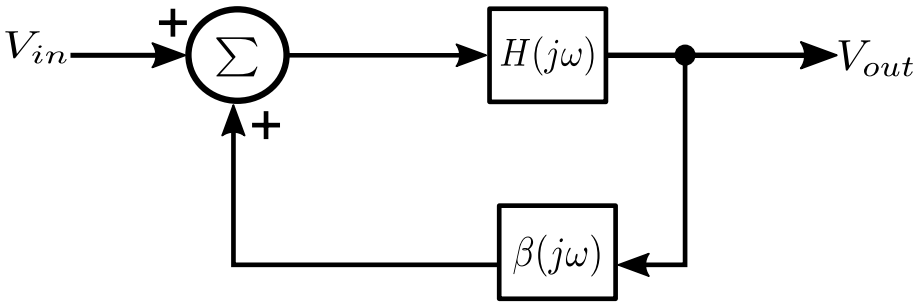

Figure 3: Positive feedback system.

Mathematically, the above system can be expressed as:

$$V_{out} = V_{in}H(j\omega) + V_{out}H(j\omega)\beta(j\omega) \tag{5}$$

where V_{in}, V_{out}, $H(j\omega)$ and $\beta(j\omega)$ are the input voltage, output voltage, open-loop gain and feedback transfer function of the system respectively. On re-arranging the like-terms of Eq. (5), the closed loop gain of the system is obtained as:

$$\frac{V_{out}}{V_{in}}\Big(j\omega\Big) = \frac{H(j\omega)}{1 - \beta(j\omega)H(j\omega)} \tag{6}$$

A linear circuit oscillates when it becomes unstable. The poles of the transfer function must lie on the right-half plane of the complex plane. Therefore, the system becomes unstable and starts oscillating when the magnitude of the open loop gain is:

$$|\beta(j\omega)||H(j\omega)| \geq 1 \tag{7}$$

and, the total phase shift around the loop is:

$$\angle(j\omega)H(j\omega) = 2k\pi, \qquad k = 0, 1, 2, .., .., n \tag{8}$$

Eq. (7) and Eq. (8) are the two most popular expressions called Barkhausen criterion for oscillation, which states that the loop gain must be unity and the total phase shift around the loop is 0 degree or integer multiple of 2π.

2.3 Phase Noise

Phase noise is a key specification of an oscillator that defines its spectral purity. An ideal oscillator with some initial energy given would always produce perfect sinusoidal output at the desired frequency of form [6]:

$$x(t) = A_0 \cos(\omega_0 t) \tag{9}$$

where A_0 is the amplitude of an oscillator output signal respectively. In reality, however, the output of an oscillator shows fluctuation in both phase and amplitude due to the noises generated by the oscillator devices. Due to the amplitude limiting mechanism present in all the oscillators, amplitude fluctuations are greatly attenuated and hence, phase noise dominates. So, the performance of an oscillator is mainly determined by its phase perturbation at the zero crossings of the output signal that occurs at an integral multiple of $2\pi/\omega_0$ [6, 7]. With addition of the phase noise, the output of the oscillator as expressed in Eq. (9) becomes:

$$x(t) = A_0 \cos[\omega_0 t + \varphi(t)] \tag{10}$$

where the term $\varphi(t)$ is a small random phase fluctuations at the zero crossings of the output signal, and is called phase noise. So, the instantaneous frequency is:

$$\begin{aligned} \omega(t) &= \frac{d}{dt}[\omega_0 t + \varphi(t)] \\ &= \omega_0 + \frac{d\varphi}{dt} \end{aligned} \tag{11}$$

which implies that the random fluctuation in the phase results in random fluctuations in the frequency. Figure 4 shows the power spectrum in case of ideal and real oscillator respectively.

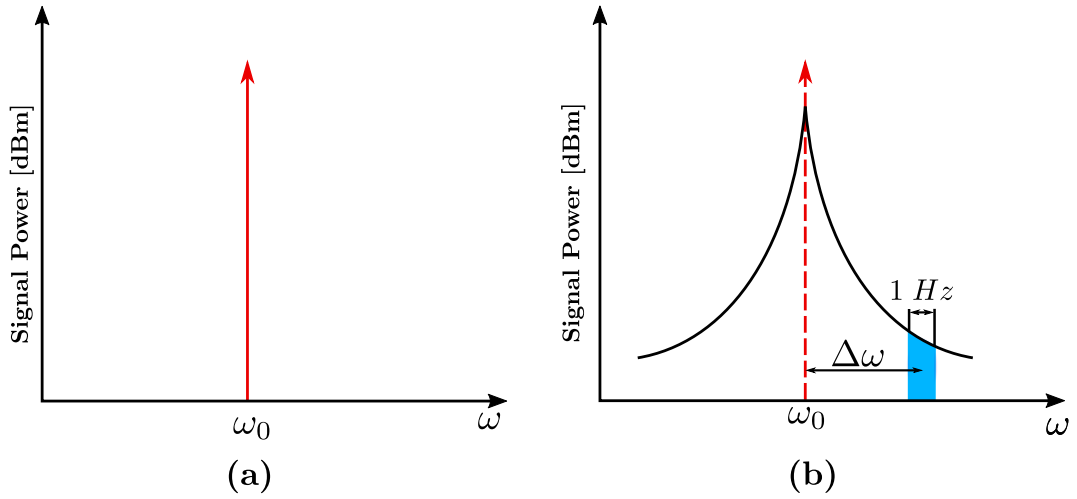

Figure 4: (a) Spectrum of ideal oscillator. (b) Spectrum of realistic oscillator.

In electronic circuits analysis and design, one of the challenging task is an analytical description of an oscillator phase noise. Various simulation and analysis techniques in

both frequency domain and time domain have been developed in the last few decades to realize the phase noise of an oscillator accurately. This challenge is due to the fact that small signal approximation for noise analysis does not work well for realizing the phase noise of the oscillators. Also, it is difficult to extract the parameters with precision in current technologies to accurately approximate the large signal model of a transistor.

One of the most preferred formula to predict the phase noise of an oscillator is given by the Lesson's model (Figure 5) which still continues to be popular 60 years later as expressed below.

$$\mathcal{L}_{\Delta\omega} = 10\log_{10}\left[\frac{2FkT}{P_{sig}}\left\{1+\left(\frac{\omega_0}{2Q\Delta\omega}\right)^2\right\}\left(1+\frac{\Delta\omega_{1/f^3}}{|\Delta\omega|}\right)\right] \tag{12}$$

where $\mathcal{L}_{\Delta f}$ is phase noise of the oscillator in dBc/Hz, F is a fitting parameter introduced by Lesson [8], T is absolute temperature, k is Boltzmann's constant, $\Delta\omega_{1/f^3}$ is flicker noise corner frequency, ω_0 is carrier frequency, P_{sig} is carrier power and $\Delta\omega$ is offset from the carrier frequency. Eq. (12) suggests that the phase noise has proportional relationship with the Q of the resonator and the output signal power of the oscillator.

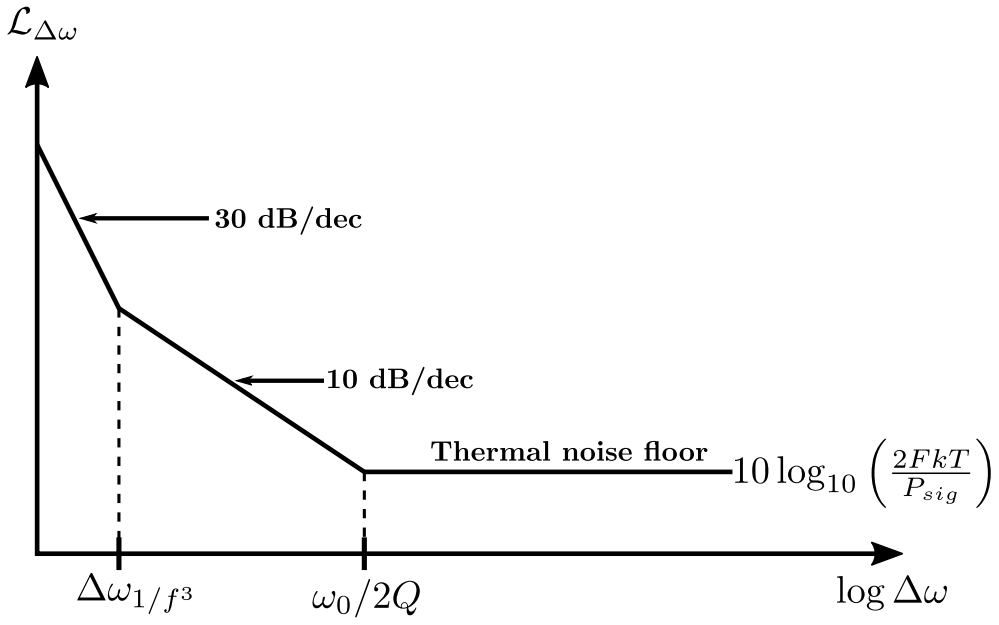

Figure 5: Lesson's phase noise model.

Phase noise is specified as the ratio of the noise power at an offset frequency $\Delta\omega$ from the carrier frequency ω_0 to the carrier power P_{sig} over 1 Hz bandwidth. It is generally expressed in dBc/Hz. The spectrum of phase noise consists of three components, one at the carrier frequency, representing the carrier power and two symmetrical noise sidebands of equal magnitude around the carrier at $\omega_0 + \Delta\omega$ and $\omega_0 - \Delta\omega$, which determines an oscillator phase noise [9].

2.4 Figure of Merit

Main parameters that characterizes an oscillator can be expressed thorough single formula called a figure of merit (FOM). It helps to compare different types of oscillator operating at different frequencies in more realistic way. Based on the necessity and the technology limitation, an oscillator can operate either at single frequency or at range of frequencies. Therefore, this results into the requirement of two expression for the FOM calculation. The most commonly used formula for calculating the FOM of an oscillator operating at single frequency is given by [9]:

$$FOM_1 = \mathcal{L}_{\Delta\omega} - 20\log_{10}\left(\frac{\omega_{osc}}{\Delta\omega}\right) + 10\log_{10}\left(\frac{P_{DC}}{1\ mW}\right) \tag{13}$$

where P_{DC} is the total DC power consumption of the oscillator in milliwatt (mW). Similarly, the FOM expression with tuning range TR included is given by [10]:

$$FOM_2 = 10\log\left(\frac{kT}{P_{DC}}\left(\frac{TR}{\Delta\omega}\right)^2\right) - \mathcal{L}_{\Delta\omega} \tag{14}$$

2.5 Classification of Oscillators

There are varieties of oscillators available based on the principle of oscillation, performance capability in RF environment and oscillation frequency band [11]. Mainly, oscillators can be categorized into two fundamental types, namely waveform-based oscillators and resonator-based oscillators on the basis of their oscillation method. Waveform-based oscillators generate triangular or square wave while the output waveform of resonator-based oscillators is usually sinusoidal [12]. The clear illustration of the oscillators classification is shown in Figure 6 below.

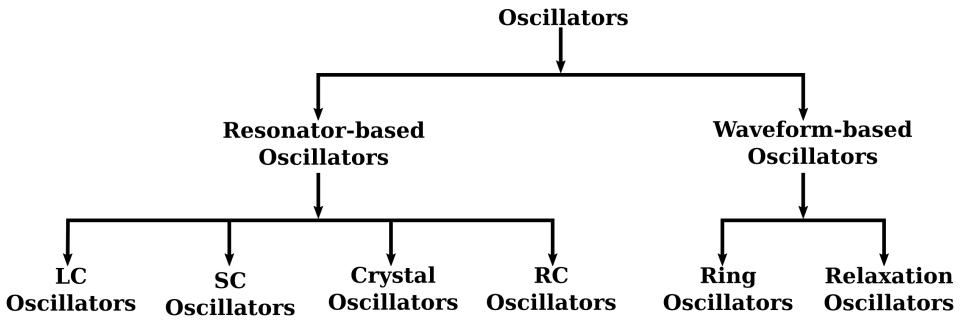

Figure 6: Classification of oscillators.

Based on the tuning mechanism, resonator-based oscillators can be further classified into RC oscillators, crystal oscillators, switched-capacitor (SC) oscillators and LC oscillators. RC oscillators do not have any inductors. They use resistor capacitance for oscillation frequency and are useful for audible frequencies. They can be further

divided into Wien Bridge oscillators, twin-T oscillators and RC phase shift oscillators. Similarly, LC oscillators can be further classified into Colpitts oscillators, Clapp oscillators, cross coupled oscillators, Hartley oscillators and Armstrong oscillators [12, 13].

Different oscillators relies on certain technique for frequency tuning. For example, variable capacitors are employed in LC oscillators for frequency tuning, whereas the tuning depends upon current steering technique in case of ring oscillators. Ring oscillators can be fully integrated on chip and has better phase noise performance than relaxation oscillators but not as good as LC oscillators. The phase noise performance of the LC oscillators are even comparable to the crystal oscillators in some applications. LC oscillators have high quality factor due to its tendency to store energy whereas RC-based oscillators have almost unity Q which results into very low phase noise performance [12].

Besides, LC oscillators due to its good phase noise performance at high frequencies and ring oscillators due to its simplicity and integrability have become dominant choice in radio frequency integrated circuits (RFICs). In addition, cross coupled oscillators also popularly known as negative resistance oscillators and Colpitts oscillators are the two most fabricated LC oscillators in ICs [4]. It can be said that ring oscillators, Colpitts oscillators and cross-coupled oscillators are the three main categories of the integrated oscillators. Therefore, these three oscillators being the excellent choice for ICs are discussed in this document.

2.5.1 Cross-Coupled Oscillator

Cross-coupled oscillators are most commonly used oscillators in RF applications because of its differential nature, simpler implementation and good phase noise performance. In addition, differential topology facilitates direct integration with the balanced circuits like double balanced mixers that require differential inputs. A cross coupled oscillator is composed of a LC resonator that controls frequency and an active circuit that generates energy. The active circuit can be realized either with heterojunction bipolar transistor (HBT) topology, or n-type metal-oxide-semiconductor (NMOS) topology or p-type metal-oxide semiconductor (PMOS) topology or complementary metal-oxide-semiconductor CMOS topology.

A pair of BJTs/MOSFETs in differential configuration with their base/gates connected to one another collector/drain generates negative resistance. On connecting this circuit in parallel to the LC tank cancels the energy loss due to the resonator. Each transistor acts as a tuned amplifier and provides π phase shift at oscillation frequency. The feedback contributes additional π phase shift making total phase shift of 2π around the loop which fulfills the Barkhausen criterion for oscillation. The resultant output signal at the differential terminals are 180° out of phase. Figure 7 shows an example of BJT cross coupled oscillator.

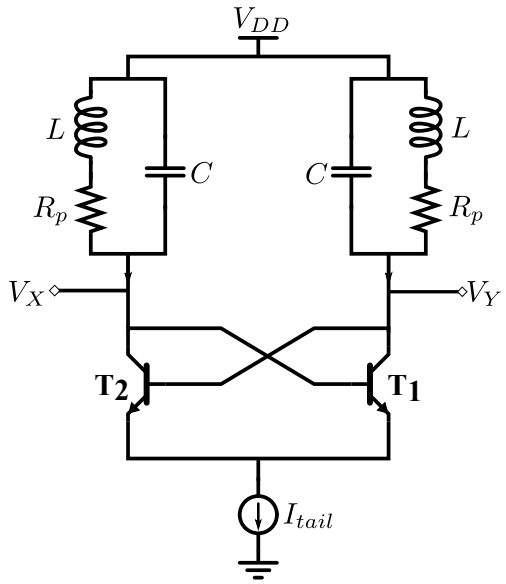

Figure 7: BJT cross coupled oscillator.

The oscillation frequency and required negative resistance for oscillation can be found by drawing equivalent small signal model of Figure 7 as shown below.

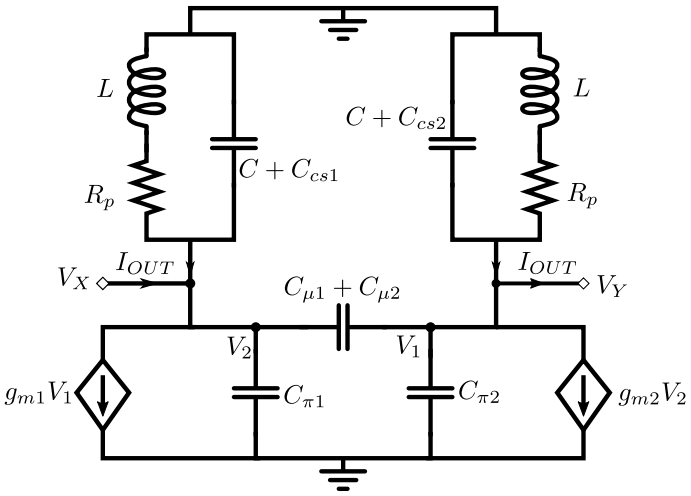

Figure 8: Small signal model of BJT cross-coupled oscillator.

Referring Figure 8, the output admittance Y of the oscillator can be expressed as a function of differential voltages V_X, V_Y and current I_{OUT} as:

$$Y = \frac{I_{OUT}}{V_X - V_Y}$$

$$= \frac{g_{m1}V_1 + \left[\frac{1}{R_p} + j\omega(C + C_{cs1} + C_{\pi1}C_{\mu1} + C_{\mu2}) + \frac{1}{j\omega L}\right]V_2 - j\omega(C_{\mu1} + C_{\mu2})V_1}{V_X - V_Y} \tag{15}$$

where $C_{\mu 1}$, $C_{\mu 2}$ are base-collector , $C_{\pi 1}$, $C_{\pi 2}$ are base-emitter, C_{cs1}, C_{cs2} are collector-substrate capacitances, g_{m1}, g_{m2} are transconductances of the transistors T_1 and T_2 respectively. Considering the symmetry of the circuit, Eq. (15) becomes:

$$Y = \frac{g_m V_1 + \left[\frac{1}{R_p} + j\omega(C + C_{cs} + C_\pi + 2C_\mu) + \frac{1}{j\omega L}\right] V_2 - j2\omega C_\mu V_1}{V_X - V_Y} \tag{16}$$

According to the Kirchhoff's law, the current entering the node must be equal to the current leaving the node. This holds true if:

$$\begin{aligned} g_m V_1 + \left[\frac{1}{R_p} + j\omega(C_\pi + C + C_{cs} + 2C_\mu) + \frac{1}{j\omega L}\right] V_2 - j2\omega C_\mu V_1 \\ = -g_m V_2 + \left[\frac{1}{R_p} + j\omega(C_\pi + C + C_{cs} + 2C_\mu) - \frac{1}{j\omega L}\right] V_1 + j2\omega C_\mu V_2 \end{aligned} \tag{17}$$

On simplification, Eq. (17) reduces to:

$$V_X = -V_Y \tag{18}$$

From Eq. (16) and Eq. (18), we get;

$$Z = -\frac{g_m}{2} + \frac{1}{2R_p} + j\left[\omega\left(\frac{C + C_\pi + C_{cs}}{2} + 2C_\mu\right) - \frac{1}{\omega L}\right] \tag{19}$$

At resonance, the imaginary part of Eq. (19) goes to zero. Therefore, the oscillation frequency is obtained as:

$$\omega_{osc} = \frac{1}{\sqrt{L(C + C_{cs} + C_\pi + 4C_\mu)}} \tag{20}$$

And, for oscillation to occur, the real part of Eq. (19) must go to zero due to the cancellation of the tank loss by the active circuit. Thus,

$$g_m = \frac{1}{R_p} \tag{21}$$

The oscillator becomes marginally stable when $g_m = 1/R_p$ which results in only desirable output. However, in practice, any small deviation in the g_m leads to a decaying or growing oscillation. So, the oscillators are generally designed with $g_m > 1/R_p$ that results into growing oscillation. On the other hand, the growing oscillation is limited by the g_m, which in practical implementation cannot draw infinite amount of power. Besides, the amplitude of oscillation depends on the nonlinear characteristics of the active circuit [4]. The oscillation amplitude V_{osc} at each output terminal of the cross-coupled oscillator as depicted in Figure 7 can be approximated as a function of tail current I_{tail} (bias current) and R_p as:

$$V_{osc} \approx \frac{2}{\pi} I_{tail} R_p \approx I_{tail} R_p \tag{22}$$

2.5.2 Ring Oscillator

Ring oscillators are formed by cascading N number of gain or delay stages. Each delay stage is composed of inverters that can be realized with currently existing high performance CMOS/BiCMOS technology. The output of each stage is connected to the input of the next stage, and the output of the final stage is connected to the input of the first, forming the closed loop system. The total number of stages used and the delay in each stage determines the oscillation frequency of an ring oscillator. For an N number of stages, the oscillation frequency of the ring is given by:

$$f_{osc} = \frac{1}{2Nt_d} \tag{23}$$

where t_d is the propagation delay at each stage. Eq. (23) implies that the oscillation frequency is mainly the function of propagation delay as N is constant for a fixed circuit. This makes the delay time the most important parameter for the study of ring oscillators. The oscillation frequency can be controlled by controlling the delay of each stage in the ring. One way to control the delay is to limit the current available for charging and discharging the load capacitors at the output of each stage. Ring oscillators are available in both single-ended and differential topology as shown in Figure 9 below.

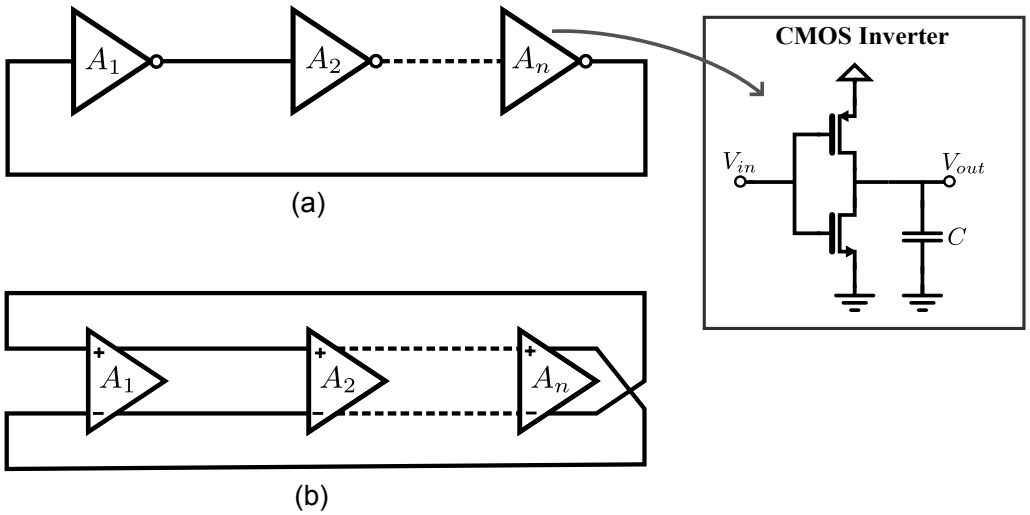

Figure 9: (a) Single-ended ring oscillator. (b) Differential ring oscillator.

Each stage in the ring adds phase shift of π/N to the signal, which means the total phase shift of π is provided by the ring. The additional phase shift of π to satisfy the Barkhausen criterion (Eqs. (7) and (8)) for a sustained oscillation is obtained from the feedback configuration. A single-ended ring oscillator requires odd number of stages for an oscillation to occur. On the contrary, the differential topology can have either an odd or even number of stages. Since the signals of both phases are available in differential configuration, the oscillation criterion can be fulfilled by swapping the feedback lines [14].

One of the main advantage of the ring oscillators is that it can be realized fully with active devices without requirement of any passive components which makes it highly preferable candidate in the integrated RF oscillators. On the contrary, the phase noise is high due to the lack of passive resonant components [15].

2.5.3 Colpitts Oscillator

Colpitts oscillator is a subclass of LC oscillator that consists of a negative transconductance stage and a resonator. The resonator consists of a pair of capacitors as a voltage divider and an inductor in parallel with these capacitors. It can be designed with just only one transistor either in common base or common emitter configuration. The common emitter configuration is usually not desired due to the requirement of a large RF choke and capacitors that are not generally available in IC technology. In addition, it also suffers form the Miller effect as neither the base nor the collector is grounded [1]. Figure 10 shows the common-collector and common base configuration of the Colpitts oscillator.

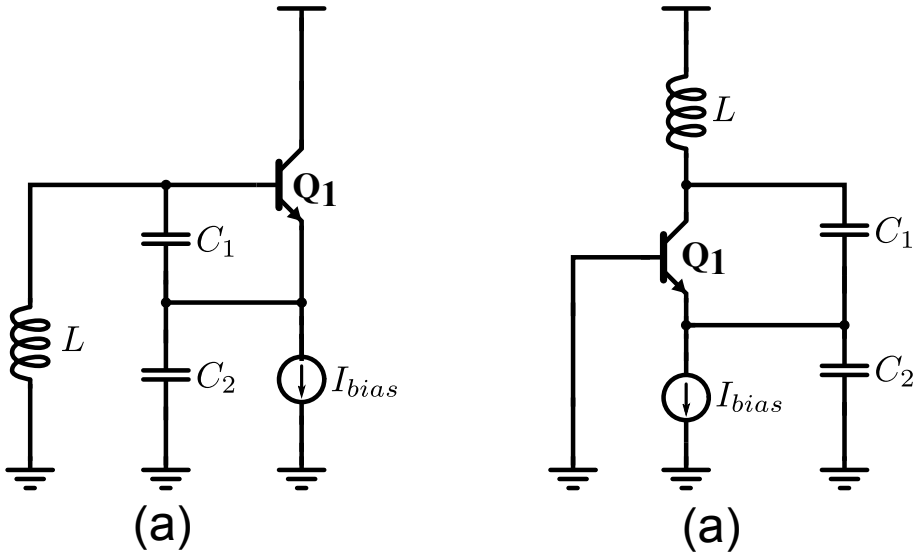

Figure 10: Colpitts oscillator: (a) Common-collector configuration. (b) Common-base configuration.

Each capacitor provides phase shift of $\pi/2$, hence total phase shift of π. The transconductance stage provides additional phase shift of π, satisfying the Barkhaunsen phase criterion for oscillation. The oscillation frequency is given by:

$$\omega_{osc} = \frac{1}{\sqrt{L\left(\frac{C_1 C_2}{C_1 + C_2}\right)}} \tag{24}$$

The output voltage is generated across C_1 and the feedback voltage is generated across C_2. The ratio between the capacitors C_1 and C_2 determine the amount of

feedback required for oscillation and is called feedback fraction. The feedback fraction, β is therefore:

$$\beta(j\omega) = \frac{V_{C_1}}{V_{C_2}} = \frac{C_2}{C_1} \tag{25}$$

Substituting $\beta(j\omega)$ from the above equation in Eq. (7), the required condition for oscillation is obtained as:

$$|H(j\omega)| \geq \frac{C_1}{C_2} \tag{26}$$

Eq. (26) implies that the voltage gain of the amplifier must be greater than or equal to the feedback factor β for an oscillation to occur. The negative resistance generated when seen from the resonator is:

$$R = -\frac{g_m}{\omega_{osc}^2 C_1 C_2} \tag{27}$$

Eq. (27) implies that larger negative resistance can be generated using small capacitors and large transconductance. However, it is not possible to realize small capacitance due to the parallel junction capacitance of the transistor. The Colpitts oscillator consumes more current than the cross coupled oscillator to generate the same negative transconductance. It is because the minimum voltage gain required for a Colpitts oscillator to oscillate is [1, 16]:

$$g_m R_p \geq 4 \tag{28}$$

2.6 summary

The fundamental theory of oscillators and its performance parameters along with the brief description of the most commonly used integrated oscillators, ring oscillators, cross-coupled oscillator and Colpitts oscillator have been discussed in this section. Among all, differential LC oscillators with cross-coupled topology are most widely preferred topology due its robust operation and ease of implementation.

3 Injection Locking of Oscillators

Any oscillatory systems in the nature with same or nearby frequencies tend to oscillate with the similar frequency when the coupling between them is quite strong enough. As a result, one of the systems capture the frequency of another, and starts oscillating at the same frequency. For example, two pendulums oscillating at different frequencies hanged on the same string tend to oscillate at the same frequency over time due to the coupling between them through the string. In electronics, injection locking occurs when an oscillator with certain natural frequency is injected by an external signal with enough power level that has a frequency close to or equal to the natural frequency of that oscillator. Upon injection, the oscillator follows the phase and frequency of the injected signal and tends to oscillate with the frequency of the injected signal maintaining constant phase difference between them [6, 17].

For an LC oscillator to be injection locked at different frequency than the resonance frequency, the tank must be supplied with net reactive current by the injection current. This is because the tank does not appear as open circuit as in case of resonance, therefore, current must be drawn [18]. Injection locking can occur on a fundamental frequency itself or an integral multiple or submultiple of the fundamental frequency. An oscillator will always try to oscillate at the injection frequency by introducing enough phase shift when the locking signal is slightly different from the oscillating signal. In case, if the oscillator bears no phase difference with the injected signal, the oscillator is said to be synchronized to the injection signal [6, 17, 19–21].

The traditional PLL with currently existing technology suffers from large chip area and high power consumption. The LC oscillators have low tuning range, occupy large area and provide decent phase noise performance. On the contrary, the ring oscillators have very poor phase noise performance [22]. Injection locking proved to be useful in various applications such as quadrature generation [23, 24], oscillators with finer phase separations [25], and frequency division [26]. Injection locking allows the operation of circuits at mm-frequencies with low power consumption, providing wide locking range and occupying smaller chip area. In addition, it dramatically reduces the phase noise of the oscillator, since the zero crossings of the oscillator are corrected periodically by the low noise injection source [27]. Besides, the oscillator signal can be fined tuned to the desired frequency that may have shifted to the nearby frequency due to the process variations.

3.1 Theoretical Background on Injection Locking

Injection locking is a technique of transforming the low quality signal to the signal of high spectral purity. Injection locking phenomenon, first realized by the Dutch scientist Christian Huygens has been studied tremendously over the years by Kurokawa [19], Paciorek [21], Adler [17], Razavi [6], Mirzaei [20] and others. A lot of efforts have been made to explain the phase noise shaping phenomenon, accurate prediction of the LR and behaviour of the oscillators under injection of small and

large signals. Although the models presented in [17, 19–21, 28] are approximate, they are useful for predicting the behaviour of the ILO.

The Locking Range

The frequency range over which the oscillator locks to the external signal injected is called LR of an ILO. If the injection frequency lies outside of the LR, the oscillator goes under pulling phenomena [28]. Figure 11 shows the conceptual diagram of the ILO as used by Razavi to describe the injection locking phenomenon. Based on the figure, the oscillator can be interpreted geometrically and the lock range can be derived on that basis. Here, we take the Razavi approach to derive the locking range of the ILO under the sinusoidal injection.

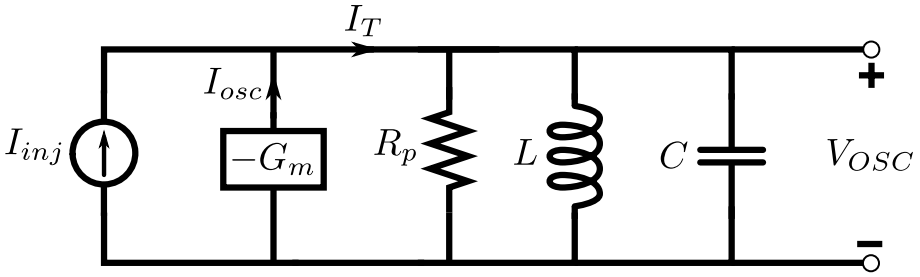

Figure 11: Conceptual diagram of injection locked oscillator.

Before moving forward to the actual mathematics of the injection locking, let's derive the phase shift introduced by the second order parallel LC tank nearby resonance frequency. The impedance Z_{LC} of the second order parallel RLC is:

$$Z_{RLC} = \frac{1}{\sqrt{\frac{1}{R_p} - j\left(\omega C - \frac{1}{\omega L}\right)}} \tag{29}$$

where ω is any arbitrary frequency offset from the natural frequency of the tank circuit. The phase shift introduced by the tank near its natural frequency is:

$$\begin{aligned} \tan\phi &= -R_p\left(\omega C - \frac{1}{\omega L}\right) \\ &= \frac{R_p}{\omega L}\left(1 - \omega^2 LC\right) \end{aligned} \tag{30}$$

Substituting $Q = R_p/\omega L$ and $1/\omega_0^2 = LC$ in Eq. (30) yields,

$$\tan\phi = \frac{Q}{\omega_0^2}\left(\omega_0^2 - \omega^2\right) \tag{31}$$

Approximating $\omega_0^2 - \omega^2 \approx 2\omega_0$, we get;

$$\tan\phi \approx \frac{2Q}{\omega_0}(\omega_0 - \omega) \tag{32}$$

At resonance frequency, the phase angle between the oscillating voltage $\vec{V}_{osc}$, the tank current $\vec{I}_{tank}$ and the oscillating current $\vec{I}_{osc}$ is zero i.e., they are perfectly aligned with each other. But, when an external signal $\vec{I}_{inj}$ with proper amplitude and frequency is injected, the phase angle is introduced between $\vec{I}_{osc}$ and $\vec{I}_{inj}$ such that $\vec{I}_{tank}$ becomes resultant of the two signals. The $\vec{I}_{osc}$ remains aligned with the $\vec{V}_{osc}$. Also, it is obvious from Figure 11 that tank current is sum of the injection current and the oscillating current [28]. Thus,

$$\vec{I}_{tank} = \vec{I}_{inj} + \vec{I}_{osc} \tag{33}$$

The relation between $\vec{I}_{inj}$, $\vec{I}_{osc}$ and $\vec{I}_{tank}$ can be described geometrically with phasor diagram as shown in Figure 12 below.

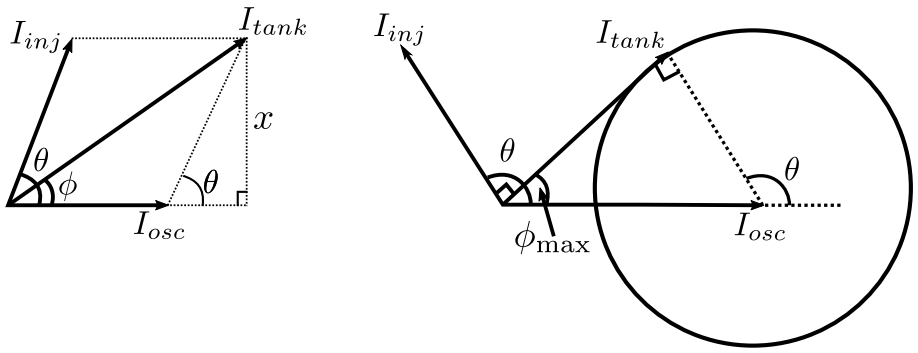

Figure 12: (a) Phasor diagram showing the relation of oscillator current, injection current and tank current. (b) Maximum allowed phase difference between the tank current and the oscillator current.

Referring to Figure 11, the oscillation amplitude can be approximated as:

$$\vec{V}_{osc} \approx Z_{tank}\vec{I}_{tank} \tag{34}$$

Similarly, the oscillating current, $\vec{I}_{osc}$ can be defined as the product of the $\vec{V}_{osc}$ and the large signal transconductance G_m as:

$$\vec{I}_{osc} = G_m\vec{V}_{osc} \tag{35}$$

Substituting $\vec{V}_{osc}$ from Eq. (34) into Eq. (35) yields,

$$\vec{I}_{osc} = Z_{tank}G_m\vec{I}_{tank} \tag{36}$$

From Figure 12(a), the phase angle ϕ between $\vec{I}_{inj}$ and $\vec{I}_{osc}$ is:

$$\phi = \angle\vec{I}_{osc} - \angle\vec{I}_{tank} \tag{37}$$

Therefore, from Eqs. (34), (36) and (37), the phase difference between the tank current and the oscillator current is:

$$\phi = \angle Z_{tank} \tag{38}$$

Eq. (38) implies that the angle between the tank current and the oscillating current is equal to the phase of the tank's impedance. This means, for $\omega \neq \omega_0$, $\vec{I}_{osc}$ must bear phase difference with $\vec{I}_{tank}$ to match the phase shift introduced by the tank such that $\vec{I}_{inj}$ form an angle θ with $\vec{I}_{osc}$ to compensate the introduced phase shift. Now, we derive the relation of ϕ with $\vec{I}_{inj}$, $\vec{I}_{osc}$ and $\vec{I}_{tank}$ using the phasor diagram as depicted in Figure 12(a). Using trigonometric identity, it can be shown that:

$$\sin\theta = \frac{x}{I_{inj}} \tag{39}$$

where x is a perpendicular line drawn form the $\vec{I}_{tank}$ on the $\vec{I}_{osc}$. Also,

$$\sin\phi = \frac{x}{I_{tank}} \tag{40}$$

From Eq. (39) and Eq. (40), we get;

$$\sin\phi = \frac{I_{inj}}{I_{tank}}\sin\theta \tag{41}$$

Using the law of cosine, $\vec{I}_{tank}$ can be expressed as:

$$\begin{aligned} I_{tank}^2 &= I_{osc}^2 + I_{inj}^2 - 2I_{inj}I_{osc}\cos(\pi-\theta) \\ &= I_{osc}^2 + I_{inj}^2 + 2I_{inj}I_{osc}\cos\theta \end{aligned} \tag{42}$$

Substituting I_{tank} from Eq. (42) into Eq. (41), we get;

$$\sin\phi = \frac{I_{inj}\sin\theta}{\sqrt{I_{osc}^2 + I_{inj}^2 + 2I_{inj}I_{osc}\cos\theta}} \tag{43}$$

As depicted in Figure 12(b), θ varies from $-\pi$ to π making a circle on full rotation. At the same time, ϕ varies from $-\pi/2$ to $\pi/2$. So geometrically, it is not possible for ϕ to change after certain $\vec{I}_{inj}$. The only parameters that continues to change on changing $\vec{I}_{inj}$ is θ. So, we differentiate Eq. (43) with respect to θ. The slope of any continuous function becomes zero at maximum and minimum value. Therefore, the maximum value allowed for $\sin\phi$ can be found from:

$$\frac{d}{d\theta}\Big(\sin\phi\Big) = 0 \tag{44}$$

which leads to the following solutions for $\cos\theta_{\max}$:

$$\cos\theta_{\max} = \begin{cases} -\dfrac{I_{osc}}{I_{inj}}, & I_{inj} \geq I_{osc} \\ -\dfrac{I_{inj}}{I_{osc}}, & I_{inj} \leq I_{osc} \end{cases} \tag{45}$$

On substituting the solutions obtained in Eq. (45) leads to the following solutions for $\sin\phi_{\max}$:

$$\sin\phi_{\max} = \begin{cases} 1, & I_{inj} \geq I_{osc} \\ \dfrac{I_{inj}}{I_{osc}}, & I_{inj} \leq I_{osc} \end{cases} \tag{46}$$

With $\sin\phi_{\max} = 1$, $\tan\phi$ goes to ∞. On the other hand, the tangent of ϕ with $\sin\phi_{\max} = I_{inj}/I_{osc}$ is:

$$\tan\phi = \frac{\sin\phi}{\cos\phi} = \frac{\sin\phi}{\sqrt{1-\sin\phi^2}} = \frac{I_{inj}}{I_{osc}} \cdot \frac{1}{\sqrt{1-\dfrac{I_{inj}^2}{I_{osc}^2}}} \tag{47}$$

Therefore, substituting $\tan\phi$ from Eq. (32) and considering $\omega_{inj} = \omega$ in the respective equation, the lock range ω_L of an ILO can be expressed as:

$$\omega_L = \omega_0 - \omega_{inj} = \frac{\omega_0}{2Q}\frac{I_{inj}}{I_{osc}} \cdot \frac{1}{\sqrt{1-\dfrac{I_{inj}^2}{I_{osc}^2}}} \tag{48}$$

where ω_{inj} is the injection frequency. Eq. (48) is for only one-sided LR. The overall LR is $\pm\omega_L$ around ω_0 [28]. On the other hand, the LR goes to infinity with $\tan\phi = \infty$, which is physically impossible. Hence, the maximum LR is obtained for:

$$\sin\phi_{\max} = \frac{I_{inj}}{I_{osc}} \tag{49}$$

As illustrated in Figure 12(b), Eq. (49) leads to the conclusion that $\vec{I}_{inj}$ makes maximum angle of 90° with $\vec{I}_{tank}$, implying maximum phase difference of $90° + \phi_{\max}$ between $\vec{I}_{inj}$ and $\vec{I}_{osc}$.

For very small injection current $I_{inj} << I_{osc}$, the lock range ω_L as depicted in Eq. (48) can be approximated as:

$$\omega_L = \frac{\omega_0}{2Q}\frac{I_{inj}}{I_{osc}} \tag{50}$$

On the basis of Eq. (48), it can be concluded that the LR depends upon the Q of the tank. For wider locking range, the Q of the tank can be decreased. But, this leads to the decreased oscillating amplitude and requires extra power to produce the required output level, which in result increases the power consumption. Another parameter that can be considered to increase the LR is the injection current I_{inj}. But, this comes in cost of the additional power dissipation.

3.2 Subharmonic Injection Locking

A free running oscillator can be locked to the N^{th} ($N = \omega_0/\omega_{inj}$) harmonic of the injected signal such that it starts oscillating at the frequency $\omega_0 = N\omega_{inj}$. When locked, the oscillator tracks down the phase noise of the injected signal and hence, the phase noise of the oscillator is highly suppressed by the factor of N^2 ($20\log_{10} N$). For this phase noise reduction to happen, N must be an integer. With N being the frequency ratio of the fundamental frequency to the injected frequency, the phase noise $\mathcal{L}_{\Delta\omega}$ of the oscillator within the LR under subharmonic injection is [27]:

$$\mathcal{L}_{\Delta\omega} = \mathcal{L}_{inj} + 20\log_{10} N \tag{51}$$

where $\mathcal{L}_{inj}$ is phase noise of the injected signal. Figure 13 is an illustration of the phase noise characteristics of an oscillator under subharmonic injection.

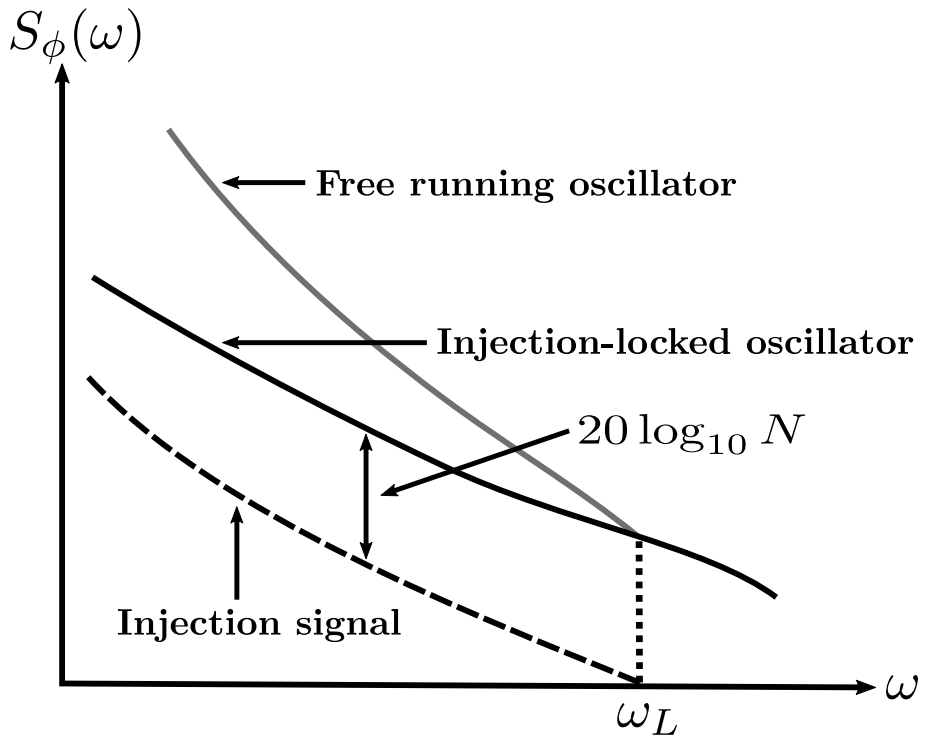

Figure 13: Subharmonically injection locked oscillator phase noise.

The effective injection current for subharmonically injection locked oscillator is I_{inj}/N [27]. Therefore, the LR as depicted in Eq. (48) becomes:

$$\omega_L = \frac{1}{N}\cdot\frac{\omega_0}{2Q}\frac{I_{inj}}{I_{osc}}\cdot\frac{1}{\sqrt{1-\dfrac{I_{inj}^2}{I_{osc}^2}}} \approx \frac{1}{N}\cdot\frac{\omega_0}{2Q}\frac{I_{inj}}{I_{osc}} \tag{52}$$

The above expression is only valid for approximating the LR of a standalone oscillator. It can be noted from Eq. (52) that the LR degrades as the N increases.

3.3 Noise-Shaping Phenomenon

One of the main characteristics of an ILO is phase noise shaping phenomenon. The ILO follows the phase noise of the injected signal. The spectral purity of the output signal from an ILO depends upon the quality of the injected signal. This is a reason for the requirement of an ILO in high frequency applications as the low phase noise signal from an oscillator can be transformed to the signal of excellent phase noise. Figure 14 shows the phase noise shaping phenomenon of an ILO.

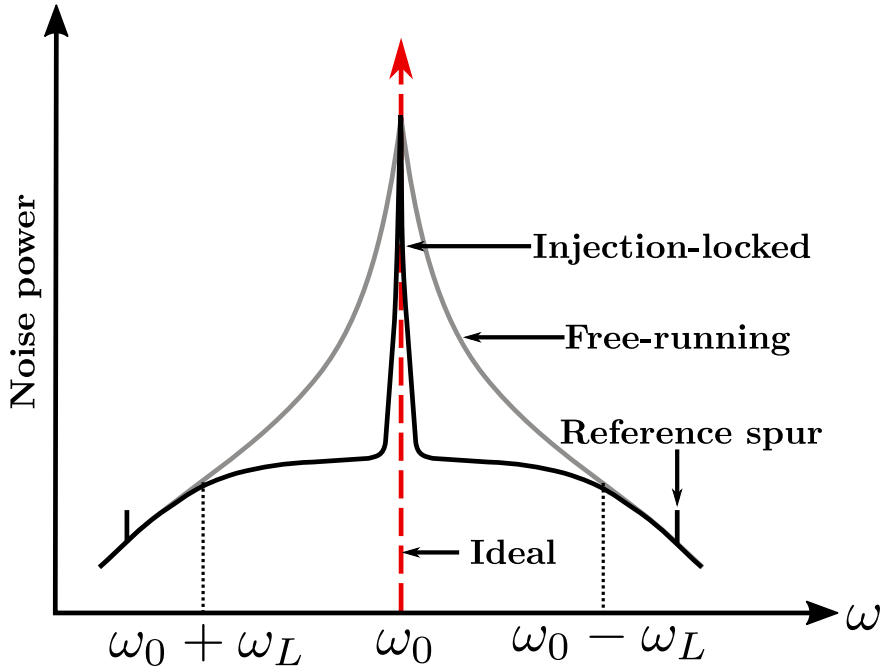

Figure 14: Phase noise shaping phenomenon in an ILO.

As depicted in Eq. (51), the phase noise shaping phenomenon is determined by the N. The phase noise shaping degrades as the N increases. Also, the phase noise follows Eq. (51) within the LR. The minimum degradation in the phase noise occurs at the center of the LR and the maximum degradation at the edges of the LR. So in practical ILOs, the main oscillation frequency is tuned at the center of the LR [27].

4 Design Description

The ILO was designed using Innovation for High Performance (IHP) Microelectronics 0.13 μm SiGe HBT BiCMOS technology under a supply voltage of 1.2 V. The ILO is composed of a pair of inductors for resonance at the desired frequency, negative resistance generator for a sustained oscillation and harmonic generator for distortion of the injected signal. The core oscillator oscillates at the single frequency and no on-chip capacitors were used for resonance at the desired frequency. The inductor resonates with the total parasitic capacitance at the output of the oscillator. Hence, the design of these devices that make the ILO are discussed in this section.

4.1 Inductor

The inductor was designed with an assistance of Mühlhaus RFIC inductor toolkit in Keysight advanced design system (ADS). The toolkit synthesizes the inductor layout provided by the technology to achieve an optimal inductance. By adjusting certain parameters in the toolkit, the spiral inductor with single turn was generated. Although, the inductance and Q was around 0.128 nH and 16.1 respectively during the initial electromagnetic (EM) simulation, the final inductance was approximately 0.13 nH with Q of 6.43. The change in the values of these parameters were due to the layout considerations which are discussed in the later section. The effective inductance of the generated inductor using the toolkit versus the frequency is shown in Figure 15 below.

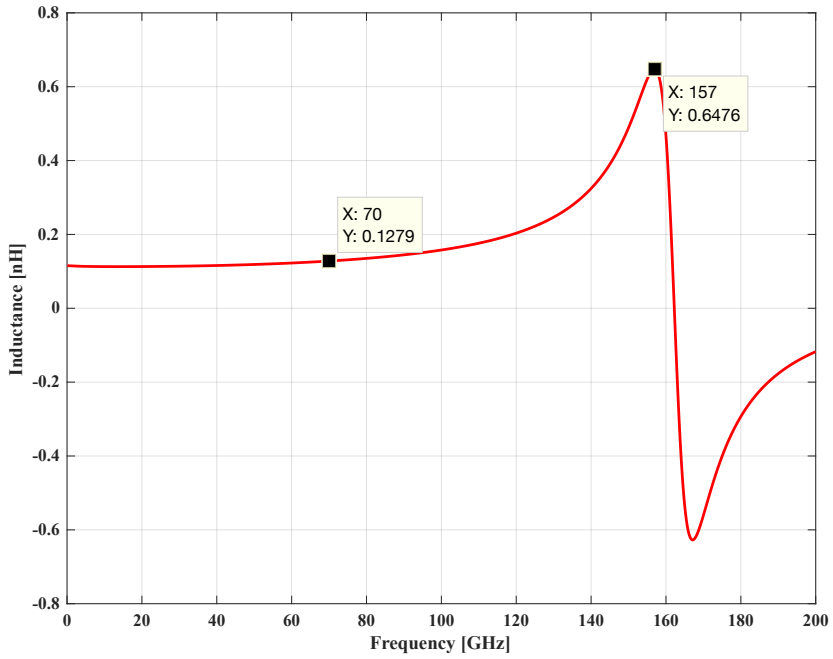

Figure 15: Effective inductance of the generated spiral inductor.

The inductor has SRF of 157 GHz which is much far away from the desired oscillation frequency. At 70 GHz, the effective series resistance R_s of the inductor is

approximately 8.75 Ω. The equivalent parallel resistance, R_p is therefore:

$$R_p = \frac{R_s^2 + X_L^2}{R_s} \approx 370.4\ \Omega \tag{53}$$

where X_L is the reactive component of the inductor impedance. Similarly, the Q of the inductor against the frequency is shown in Figure 16 below.

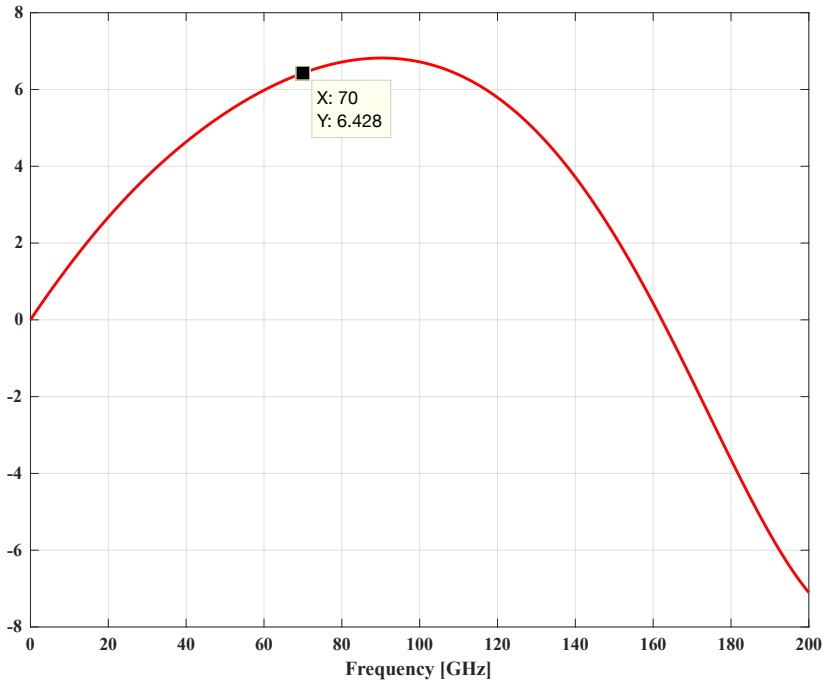

Figure 16: Q of the inductor against the frequency.

4.2 Core Oscillator

The core oscillator is a conventional cross-coupled oscillator that oscillates with the effective inductance of 0.128 nH and total parasitic capacitance of around 39.3 fF that appears at the output terminal. The parasitics of the harmonic generator also contributes to the total capacitance of the oscillator. During the initial simulations, on-chip capacitors were also used for the oscillation at the desired frequency. Since the parasitics play a critical role in mm-wave frequency, the drastic change in the oscillation frequency was observed after the post-layout simulation. Therefore, the on-chip capacitors were removed which is quite advantageous as less area is consumed. Figure 17 shows the schematic view of the designed cross-coupled oscillator.

The bias current is provided to the oscillator by the tail transistor $\mathbf{T_3}$ that mirrors the reference current of the transistor $\mathbf{T_4}$. The reference current source transistor $\mathbf{T_3}$ utilizes single multiplier, whereas the tail transistor $\mathbf{T_4}$ utilizes 8 multipliers so that lower reference current can be used. According to the theory, the active circuit

must cancel the effective series resistance of the inductor. For the oscillator as shown in Figure 17 to oscillate, each transistor $\mathbf{T_1}$ and $\mathbf{T_2}$ must have $g_m \geq 1/R_p \approx 3\ mS$. However, the equivalent g_m value does not start up the oscillation which is certain for practical circuits. Therefore, the g_m must be chosen greater than the R_p to ensure the oscillation.

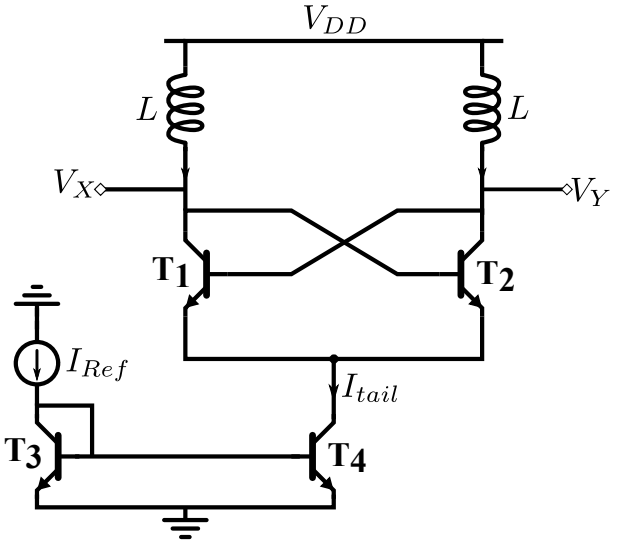

Figure 17: Core oscillator.

The oscillator starts oscillating with the tail current of 667.37 μA with very low output voltage swing of 18.5 mV. The corresponding g_m is 12.2 mS which is much greater than the required g_m value for oscillation. The large size transistors and higher bias current can be used to increase the effective g_m of the active circuit. But, this increases the parasitics and magnitude of the fundamental harmonics. Consequently, the phase noise also increases. Through the number of simulations following the sweeping of different parameters, the tail current of 2.2 mA and 2 multipliers for the active circuit transistors were fixed that provided decent phase noise performance and output voltage swing. The corresponding g_m of each transistor is 33 mS. Table 1 lists the key figure of the simulated core oscillator.

Table 1: Key figures of the core oscillator

Parameters	**Value**	**Unit**
I_{Ref}	320	μA
I_{tail}	2.2	mA
Number of Multipliers	1 for $\mathbf{T_3}$, 8 for $\mathbf{T_4}$, 2 for $\mathbf{T_1}$ and $\mathbf{T_2}$ respectively.	–
Oscillation Amplitude	373	mV
Phase Noise@1MHz	-70.12	dBc/Hz
P_{DC}	2.64	mW

4.3 Harmonic Generator

The core oscillator must be injection locked to the third and the fifth harmonics of the reference signal. The injection locking phenomenon and LR relies on the strength of the injected signal and its harmonics. The harmonics generation rely on the nonlinearities of the transistor. When biased with proper base-emitter voltage and injection power, the HBT generates all the harmonics of the injection signal. Therefore, it is very essential to study the nonlinear behavior of the HBT under different biasing conditions. The two major reasons for nonlinearities in the HBT are the nonlinear exponential current-voltage (IV) characteristic and clipping and conduction angle of the collector current [29]. Frequency triplers taking an advantage of these nonlinearities have been designed in [29–32]. Especially, [29] and [33] have clearly described the nonlinear behaviour of the HBT with mathematical derivation. Similar approach has been used in this thesis project to design the harmonic generator.

The nonlinear behavior of the HBT has been studied upon different biasing conditions with injection power of 0 dBm along with the different transistor sizing. The final simulation involves the total of 3 multipliers for the HBT. Figure 18 shows the plot of the third order and the fifth order derivative of the collector current along with the HBT IV characteristics.

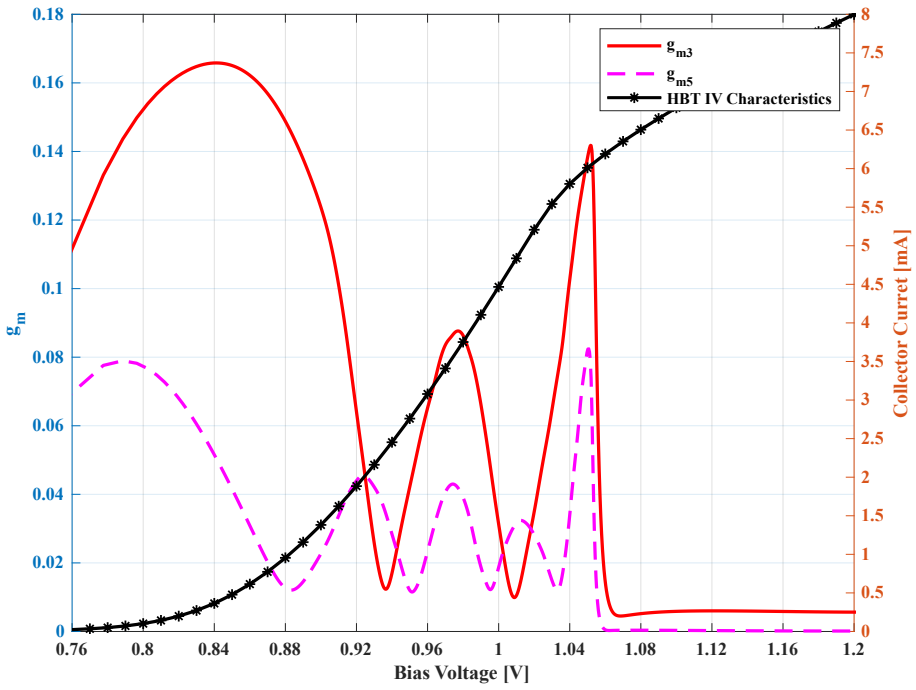

Figure 18: HBT nonlinearities with different biasing voltages.

Figure 18 shows that the HBT shows maximum nonlinearity when it turns on and near saturation region. For maximum nonlinearity and frequency conversion gain, the bias voltage of 0.83 V has been chosen that corresponds to the class AB operation. The harmonic generator is composed of a pair of BJTs in differential configuration

biased with resistor voltage divider and a coupling capacitor C_c as shown in Figure 19 below.

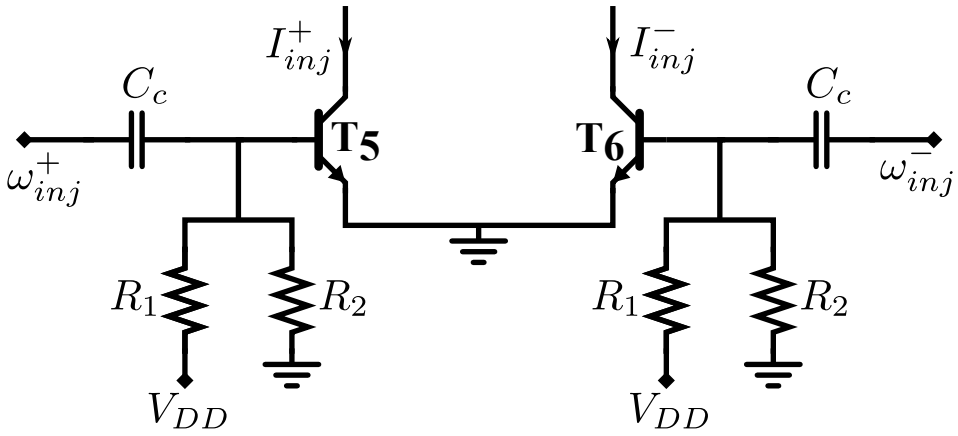

Figure 19: Harmonic Generator.

The resistor voltage divider was considered as it provides constant voltage biasing despite of the base current variation and hence, maintains the HBT nonlinearity. The values of the resistors R_1 and R_2 are 1 $k\Omega$ and 2.4 $k\Omega$ respectively. Although, in ideal case, the biasing voltage with these resistances correspond around 0.847 V, the final bias voltage of 0.83V has been achieved for the HBTs with the corresponding resistor values. This is due to the fact that the parasitics of the metal interconnects contribute to the overall resistance of the voltage divider. The coupling capacitor of 300 fF was chosen that allows the RF signals to pass into the harmonic generator while blocking the DC signals. The key figures of the simulated harmonic generator are listed in Table 2 below.

Table 2: Key figures of the harmonic generator

Parameters	**Value**	**Unit**
Bias Voltage	0.83	V
Total Number of Multipliers of Each HBT	3	–
Quiescent Current of Each HBT	1.42	mA
P_{DC}	3.4	mW

4.4 ILO Schematic and Layout Design

The direct injection topology has been utilized to inject the harmonics of the reference signal into the oscillator i.e., the outputs of the harmonic generator are directly fed into the outputs of the cross-coupled oscillator. The desired harmonic gets amplified and undesired harmonics get suppressed depending upon the frequency response and LR of the oscillator. Figure 20 shows the full schematic of the designed ILO.

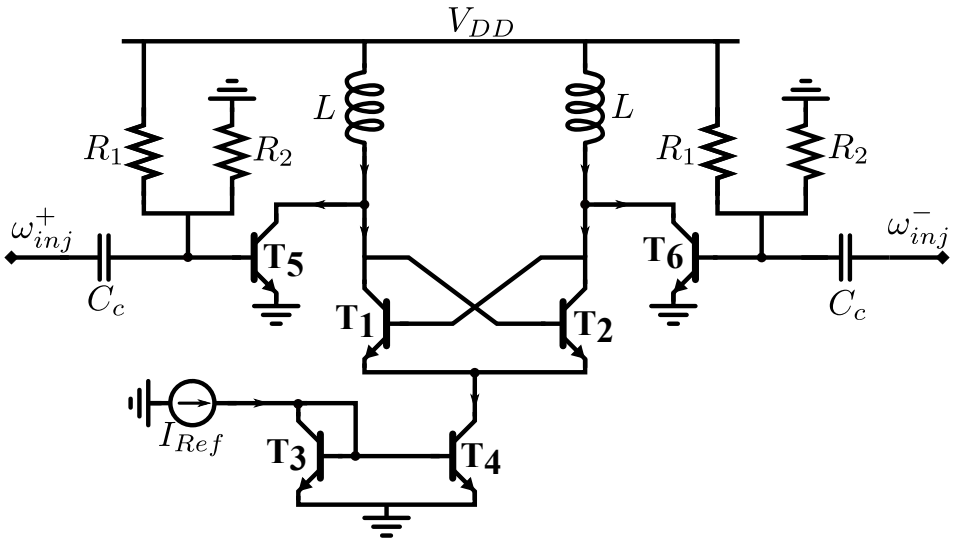

Figure 20: Full schematic of the designed ILO.

The Cadence Virtuoso layout editor was utilized to design the layout of the ILO circuit. The main challenging task during the layout design was the inductor. It was observed after the post-layout simulations that the metal interconnects of the inductor contribute significantly to its overall effective inductance and series resistance. As a result, the oscillation frequency shifted from the desired one greatly. This is the reason for the decrement of Q of the final inductance as discussed in Section 4.1. The EM simulation had to be performed number of times along with the interconnects to fine tune the oscillation frequency. Figure 21 shows the layout of the designed ILO circuit.

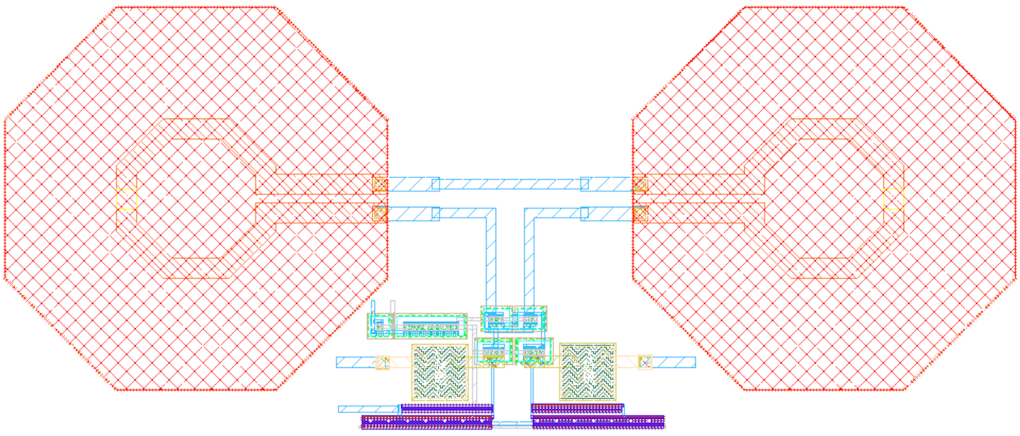

Figure 21: Layout design.

The layouts of the current mirror, harmonic generator and negative resistance generator were designed separately along with the metal interconnects and the parasitics were extracted for the simulations. Similarly, the EM simulation of the inductor was performed using the ADS Momentum and the scattering parameters file was

extracted for the simulations. After the desired oscillation frequency was achieved, each layout blocks were placed as they were designed for the pre-layout simulation verification and hence, the complete layout of the ILO was created. In addition, multiple vias were considered to decrease the resistance and increase the reliability. Also, similar orientation for the differential HBTs were considered for symmetrical reasons. The RC extraction of the layout was done and the ILO performance was evaluated whose results are presented in the later section.

5 Simulation Results

This section presents the simulation results of the ILO. The ILO was simulated using the cadence spectre and an ideal voltage, current and 50Ω RF sources have been used to provide the main supply voltage, reference current and differential signal to the circuit respectively. In addition, all the simulated results data were exported and plotted using the Matlab. Also, the discrete Fourier transform (DFT) of the transient simulated data were performed using the Matlab.

5.1 Free-running oscillator

Figure 22 shows the transient simulation and its DFT of the free running oscillator. The oscillator reaches the steady state after about 400 ps, and starts oscillating with the frequency of 71 GHz and output voltage swing of 373 mV.

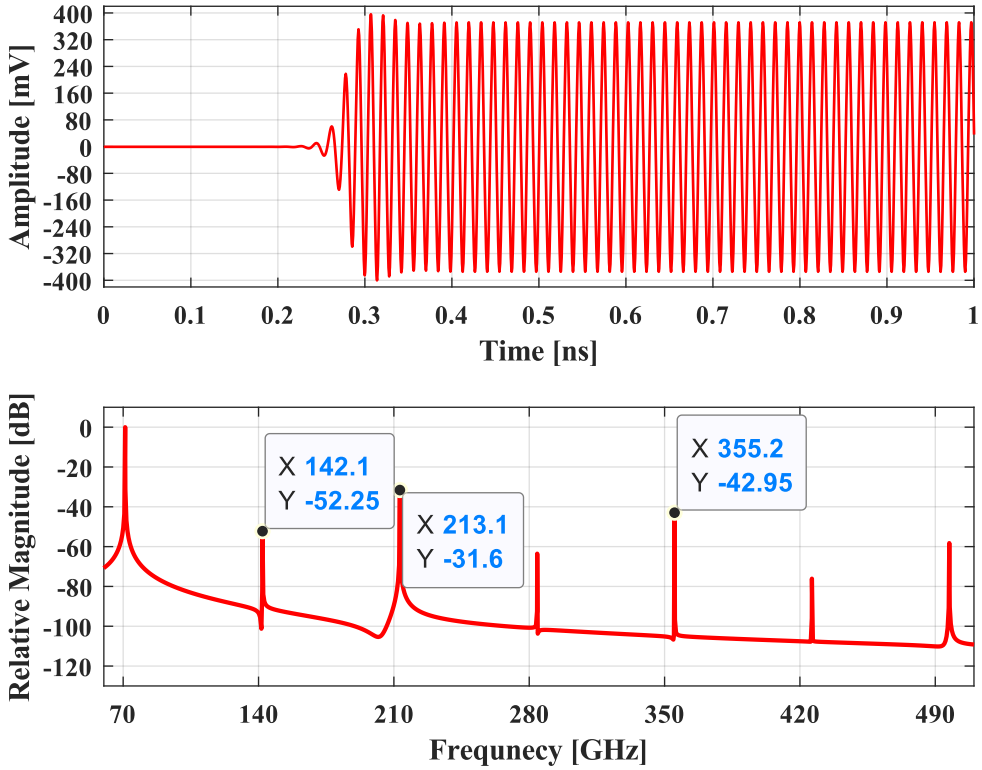

Figure 22: Transient simulation and its DFT plot of the free running oscillator.

The DFT plot shows that the even harmonics are suppressed greatly than the odd harmonics due to the differential nature of the oscillator. The magnitude of the second, third and fifth harmonics are -52.25 dB, -31.6 dB and -42.95 dB respectively below the fundamental frequency of oscillation.

Figure 23 shows the phase noise performance of the free running oscillator. At offset frequency of 1 MHz, the free-running oscillator achieves phase noise of -70.12 dBc/Hz. The corresponding FOM of the free-running oscillator is -162.93 dBc/Hz.

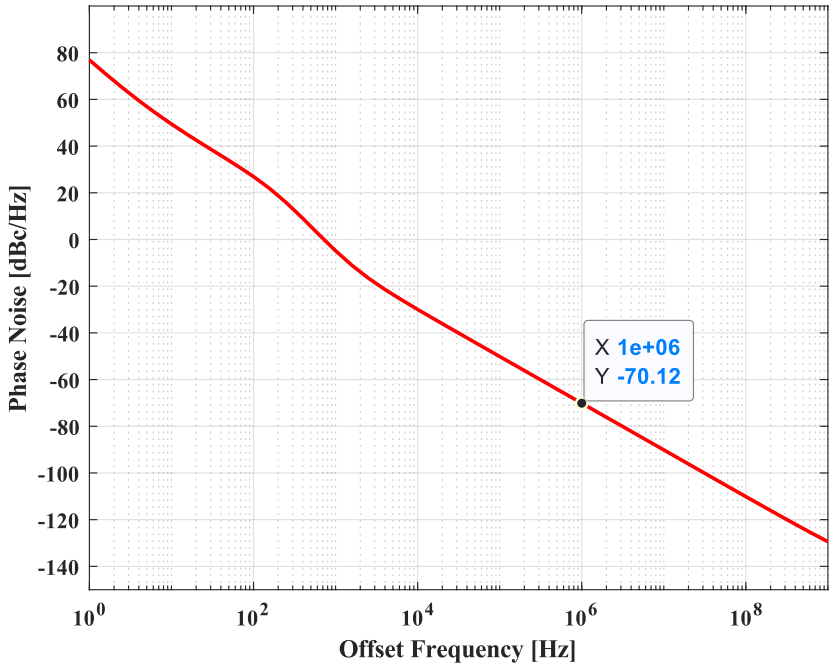

Figure 23: Free-running oscillator phase noise.

5.2 Injection-Locked Oscillator

The injection locking phenomenon was studied by injecting the 3^{rd} and 5^{th} harmonics of the injected signal. Figure 24, Figure 25 shows the injection locking to the 3^{rd} and the 5^{th} harmonics of the injection signal respectively with injection power of 0 dBm.

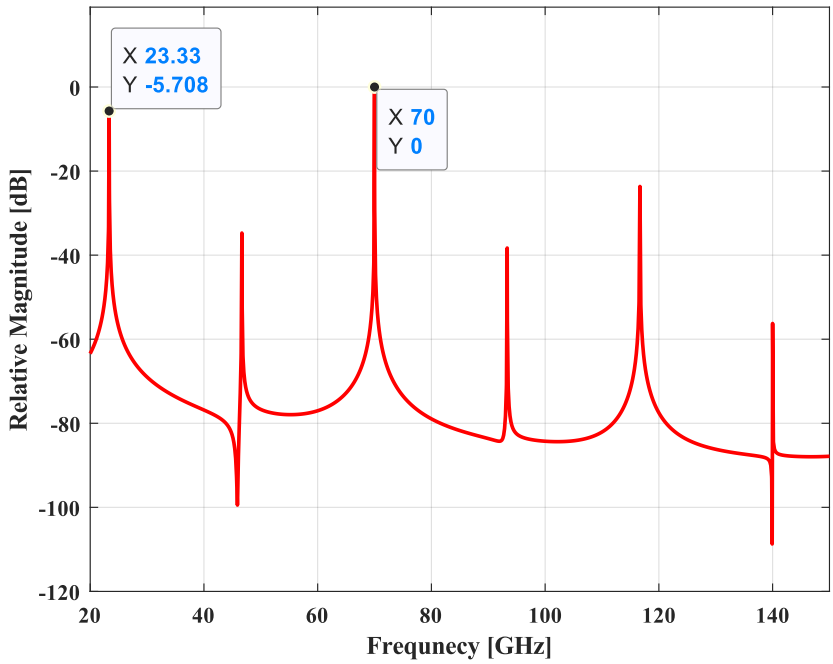

Figure 24: Third harmonic injection locking.

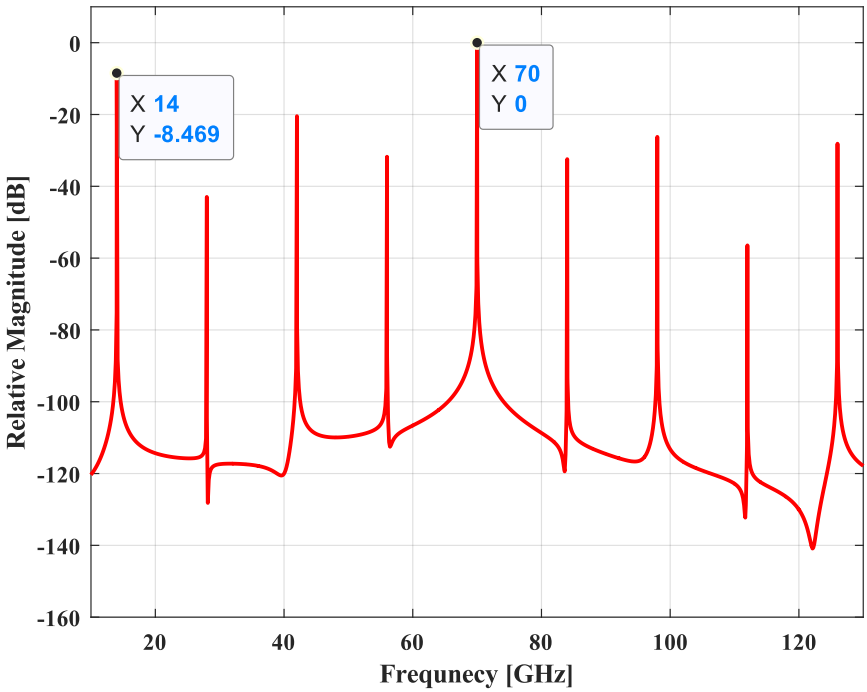

Figure 25: Fifth harmonic injection locking.

On simulation, it was found that the oscillator also locks to the 7^{th} harmonics of the injected signal with very narrow LR (Figure 29). Figure 26 shows the injection locking to the 7^{th} harmonic of the injection signal with injection power of 0 dBm.

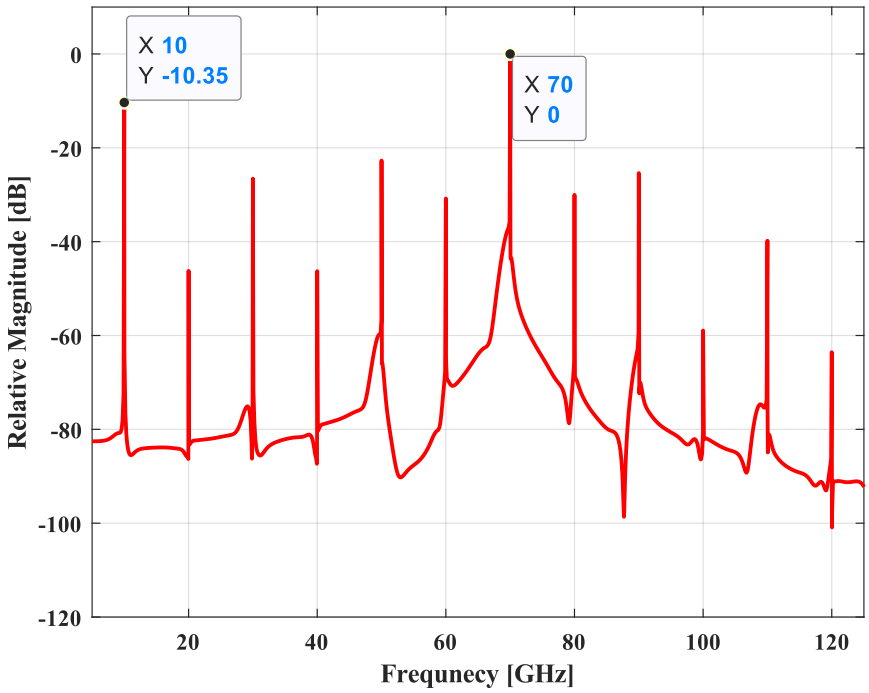

Figure 26: Injection locking to the seventh harmonic.

The magnitude of the output signal is increased under locked condition compared to the free-running oscillator due to the contribution of the injection power. Also, the reference spurs are high due to the low Q of the inductor and feedthrough the harmonic generator. To accurately determine the LR of the oscillator upon different harmonics injection, the transient simulation of the ILO was performed in wide range of frequencies with small frequency steps around the injection frequency. The locked state was found out by plotting the transient simulation and performing DFT of its data. Under locked condition, the DFT shows only the tones of the injected signal (Figures 24 to 26) with highest peak being at the locked frequency.

The oscillator goes under pulling phenomenon outside the LR. When the injection signal is close to the ω_0 and outside the LR, the oscillator goes under quasi-lock mode that consists of many tones other than the injected signal with small frequency spacing as shown in Figure 27. Similarly, when the injection signal is far from the ω_0 and outside the LR, the oscillator goes under fast beat mode. Like in quasi-lock mode, the spectrum contains many tones other than the injected signal but with larger frequency spacing as shown in Figure 28.

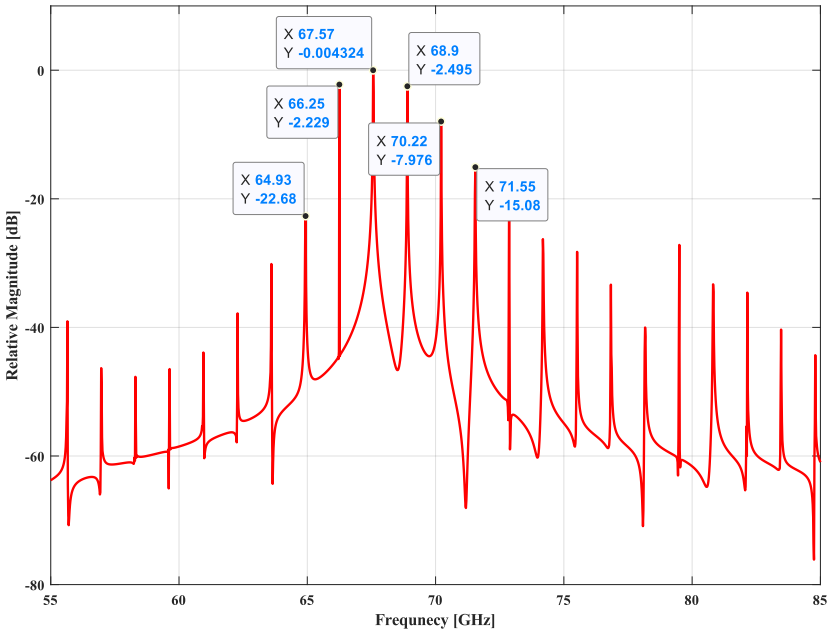

Figure 27: Oscillator under quasi-lock mode with $\omega_{inj} = 2\pi{\cdot}13.25$ GHz.

With injection power of 0 dBm, the oscillator locks the harmonics of the reference frequencies ranging from 18.9-24.5 GHz and 13.29-14.16 GHz for the third and the fifth harmonics injection respectively. The corresponding LR are 5.6 GHz for the 3^{rd} harmonics and 870 MHz for the 5^{th} harmonics injection. To verify the relation of LR with I_{inj} as depicted by Eq. (48), the injection power was swept from 0 dBm to -10 dBm, injecting the 3^{rd}, 5^{th} and 7^{th} harmonics of the reference signal. As predicted by the theory, the simulated results showed that LR decreases on decreasing the injection power and vice versa. This is because the conversion gain of the respective harmonic

decreases on decreasing the injection power. Mostly, the power of the harmonics are much weaker already after the third harmonic which results in decreased LR for higher harmonics. Figure 29 shows the LR of the ILO with various injection power and subharmonic frequencies. The minimum injection power required for injection locking to the 3^{rd} harmonic of the injection signal so that the oscillator oscillates at 70 GHz frequency is -9 dBm, and -5 dBm for the 5^{th} harmonic injection. The corresponding injection frequencies lies at the edge of the LR.

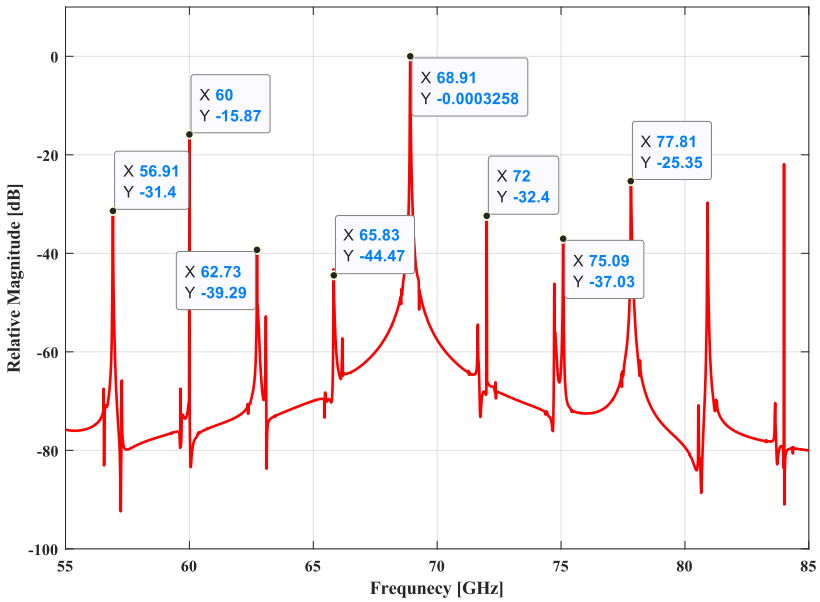

Figure 28: Oscillator under fast-beat mode with $\omega_{inj} = 2\pi{\cdot}12$ GHz.

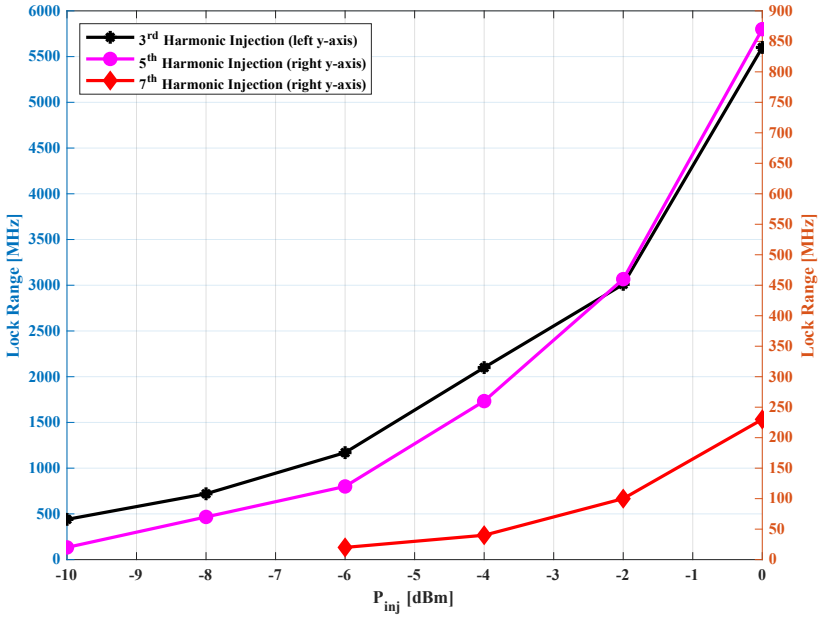

Figure 29: LR relation with input injection power.

For the phase noise simulation of the ILO, the injection source was given constant phase noise values at certain frequency offsets. Although the simulated results do not accurately predict the phase noise of the oscillator when impressed by the external signal, it helps to understand the phase noise behaviour of the ILO. In addition, it also helps to verify if the oscillator is locked to the injected signal. Under locked condition, the phase noise of the oscillator is suppressed by the factor of $20\log_{10} N$ dB as mentioned in Section 3.2. Figure 30 shows the phase noise of the input reference signal along with the output phase noise of its 3^{rd} and 5^{th} harmonics injection respectively.

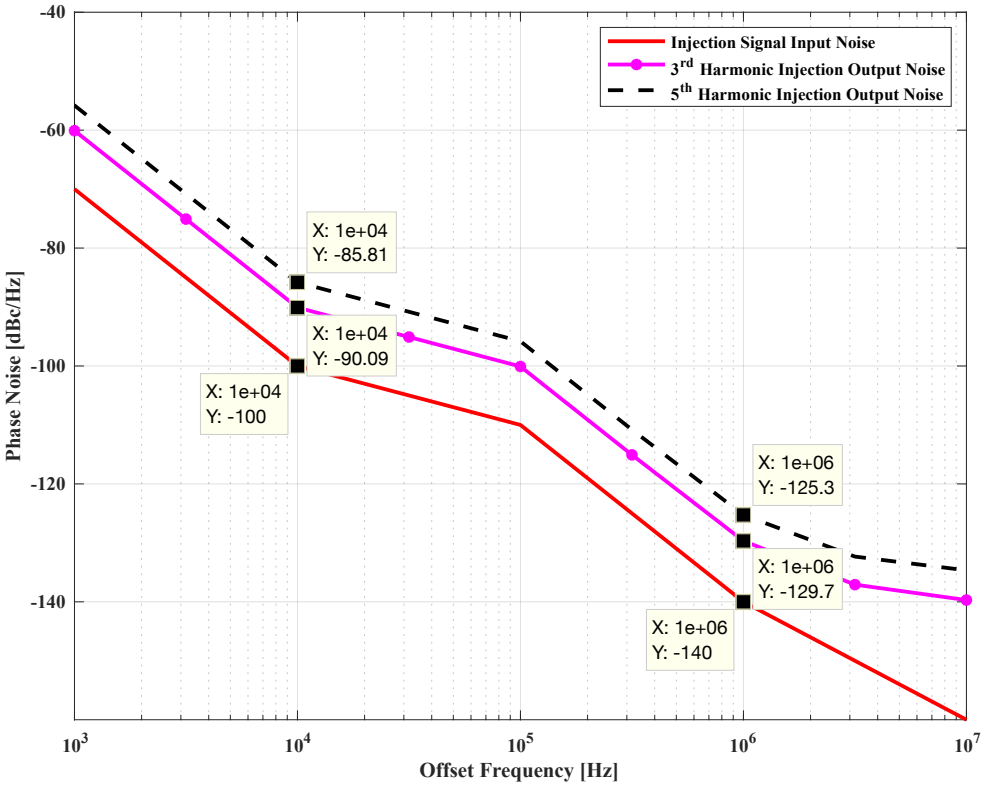

Figure 30: Phase noise characteristics of the oscillator under injection.

Figure 30 shows that the resultant output signal of the oscillator follows the phase noise of the reference signal. The phase noise degradation of 10.3 dB at 1 MHz offset frequency can seen with the third harmonic injection which is almost near to the theoretical limit of $20\log_{10} 3 = 9.54$ dB. Similarly, the phase noise degrades by 14.7 dB for the fifth harmonic injection at offset frequency of 1 MHz and approaches the theoretical limit of $20\log_{10} 5 = 13.94$ dB. The phase noise approaches almost the theoretical limit if the injection power is increased beyond 0 dBm. On the contrary, the phase phase noise degrades for the low power injection. Besides, the phase noise also approaches near to the theoretical limit with the same injection power at small offset frequency as a result of low-pass frequency response. The phase noise degradation for the third harmonic injection is already 9.91 dB at 10 kHz frequency offset which is very much close to the theoretical limit value of 9.54 dB.

5.3 Summary

Table 3 lists the achieved specification of the post-layout simulated ILO.

Table 3: Key figures of the injection locked oscillator.

Technology	$0.13\mu m$ SiGe HBT BiCMOS		
Supply Voltage	1.2 V		
Oscillating Condition	**Performance Parameters**	**Value**	**Unit**
Free-Running	Frequency	71	GHz
	Phase Noise@1MHz	70.12	dBc/Hz
	FOM@1MHz	-162.93	dBc/Hz
Injection-Locked	Divide-By-3 LR	5.6	GHz
	Divide-By-5 LR	870	MHz
	Divide-By-7 LR	230	MHz
	Injection Power	0	dBm
$\mathbf{P_{DC}}$	6.04 mW		

6 Conclusion

A mm-wave subharmonic ILO has been realized using the IHP SiGe 0.13 μm BiCMOS technology under supply voltage of 1.2 V. The final design of the ILO includes the clean design rule check (DRC) and layout vs schematic (LVS) layout that achieves injection locking to the third, fifth and even seventh harmonics of the injection signal.

The designed ILO is composed of a cross-coupled oscillator that oscillates at the frequency of 71 GHz and a differential harmonic generator that generates all the harmonics of the reference signal. The direct injection topology has been utilized to achieve the odd harmonics injection locking i.e., the differential outputs of the harmonic generator are directly injected to the differential outputs of the core oscillator. For the harmonics generation, the nonlinear characteristic of the HBT has been studied with different biasing voltages (Figure 18) and the biasing point is chosen where the HBT is most nonlinear. When biased with 0.83 V, the harmonic generator provides maximum frequency conversion gain for the required harmonics. The core oscillator consumes 2.64 mW power with tail current of 2.2 mA and the harmonic generator consumes 3.4 mW power making the total DC power consumption of 6.04 mW for the whole ILO.

The ILO achieves the LR of 7.9%, 1.22%, 0.32% for the third, fifth and the seventh harmonics injection respectively with input injection power of 0 dBm. The plot of the LR with different injection power (Figure 29) verifies the proportional relationship of LR with the injection power i.e., the LR decreases for low injection power and vice versa. The phase noise of the locked ILO follows the phase noise of the injection signal as predicted by the theory and approaches the theoretical value upon high power injection. The minimum injection power required to obtain the desired 70 GHz locked output under the third harmonic injection is -9 dBm and -5 dBm for the fifth harmonic injection. But this must be compromised with the LR and the phase noise degradation. The magnitude of the resultant output signal increases by more than 3.5 dB for all the third, fifth and the seventh harmonics injection due to the contribution of the injection power which is quite advantageous.

As a conclusion, an ILO with free-running frequency of 71 GHz, and with locking capability to the third, fifth and the seventh harmonics of the reference signal has been realized with the decent LR. The primary requirement of free-running oscillation frequency of 70 GHz can be met by increasing the bias current of the core oscillator. But, this comes in cost of increased DC power dissipation and decreased LR. On the contrary, the bias current of the oscillator can decreased, increasing the Q of the inductor at the same time to decrease the power consumption of the oscillator without degrading the LR due to the inverse proportionality relationship of the LR with the oscillating current. But, care must be taken while playing with these parameters as minimum bias current is required for sustaining the loop gain. Besides, further improvement in the design of the ILO can be done to decrease the magnitude of the reference spurs.

Furthermore, the simulation were carried out without the output buffers that may affect the main oscillation frequency and the LR due to its parasitics. Similarly, the process-voltage-temperature (PVT) analysis has not been carried out which may also affect the operation of the ILO; any variation in the supply voltage could degrade the LR greatly as the harmonic generator relies on the bias point of the HBT for harmonics generation. In addition, an ideal RF source has been used as a reference signal with input power of 0 dBm. In practical circuits, this amount of power is not possible to be transferred without using the buffer as the power gets reflected due to the impedance mismatching. As in all, the thesis work is focused mainly on studying the characteristics of an ILO rather than focusing on its practical implementation.

References

[1] J. Rogers and C. Plett, *Radio Frequency Integrated Ciruit Design*. Norwood, MA: Artech House Publisher, 2003.

[2] J. B. Hagen, *High-Frequency Electronics*, 2nd ed. New York: Cambridge University Press, 2009.

[3] C. Nguyen, *High-Frequency Integrated-Circuit Engineering*. Hoboken, New Jersey: John Wiley & Sons, Inc, 2015.

[4] H. Darabi, *High-Frequency Integrated-Circuit Engineering*. University Printing House, UK: Cambridge University Press, 2015.

[5] V. Štofanik, M. Minárik, Z. Brezović, I. Baláž, and V. Kudják, "Comparison of classical and modified wien oscillator circuits in term of existence of steady state oscillations," in *2014 24th International Conference Radioelektronika*, April 2014, pp. 1–4.

[6] B. Razavi, *RF MicroElectronics*, 2nd ed. Prentice Hall, 2011.

[7] T. H. Lee and A. Hajimiri, "Oscillator phase noise: A tutorial," *IEEE Journal of Solid-State Circuits*, vol. 35, no. 3, pp. 326–336, March 2000.

[8] D. B. Leeson, "A simple model of feedback oscillator noise spectrum," *Proceedings of the IEEE*, vol. 54, no. 2, pp. 329–330, Feb 1966.

[9] S. Voinigeschu, *High-Frequency Integrated Ciruits*. New York: Cambridge University Press, 2013.

[10] G. Cusmai, M. Repossi, G. Albasini, A. Mazzanti, and F. Svelto, "A magnetically tuned quadrature oscillator," *IEEE Journal of Solid-State Circuits*, vol. 42, no. 12, pp. 2870–2877, Dec 2007.

[11] M. Mandal and B. Sarkar, "Ring oscillators: Characteristics and applications," *Indian Journal of Pure and Applied Physics*, vol. 48, no. 2, pp. 136–145, February 2010.

[12] T. J. Rouphael, *Wireless receiver architectures and design : Antennas, Rf, Synthesizers, Mixed Signal, and Digital Signal Processing*, 1st ed. Elsevier Academic Press, 2015.

[13] C. Lin, Y. Chen, Y. Chen, and C. Chen, "Improvement of the barkhausen criterion and the implementation of an intelligent function generator," *The Journal of Engineering*, vol. 2017, no. 4, pp. 126–138, 2017.

[14] J. A. McNeill and D. S. Ricketts, *The Designer's Guide to Jitter in Ring Oscillators*. 233 Spring Street, NY: Springer Publishing Company, Incorporated, 2009.

[15] B. Razavi, "A 2-ghz 1.6-mw phase-locked loop," *IEEE Journal of Solid-State Circuits*, vol. 32, no. 5, pp. 730–735, May 1997.

[16] K. Ha, H. Ryu, J. Lee, J. Kim, and D. Baek, "g_m -boosted complementary current-reuse colpitts vco with low power and low phase noise," *IEEE Microwave and Wireless Components Letters*, vol. 24, no. 6, pp. 418–420, June 2014.

[17] R. Adler, "A study of locking phenomena in oscillators," *Proceedings of the IRE*, vol. 34, no. 6, pp. 351–357, June 1946.

[18] B. Hong and A. Hajimiri, "A phasor-based analysis of sinusoidal injection locking in lc and ring oscillators," *IEEE Transactions on Circuits and Systems I: Regular Papers*, vol. 66, no. 1, pp. 355–368, Jan 2019.

[19] K. Kurokawa, "Injection locking of microwave solid-state oscillators," *Proceedings of the IEEE*, vol. 61, no. 10, pp. 1386–1410, Oct 1973.

[20] A. Mirzaei, M. E. Heidari, and A. A. Abidi, "Analysis of oscillators locked by large injection signals: Generalized adler's equation and geometrical interpretation," in *IEEE Custom Integrated Circuits Conference 2006*, Sep. 2006, pp. 737–740.

[21] L. J. Paciorek, "Injection locking of oscillators," *Proceedings of the IEEE*, vol. 53, no. 11, pp. 1723–1727, Nov 1965.

[22] M. Li, R. D. Mason, and N. T. Abou-El-Kheir, "A fully synthesized injection locked ring oscillator based on a pulse injection locking technique," in *2017 IEEE Asia Pacific Microwave Conference (APMC)*, Nov 2017, pp. 1265–1268.

[23] C. J. M. Verhoeven, "A high-frequency electronically tunable quadrature oscillator," *IEEE Journal of Solid-State Circuits*, vol. 27, no. 7, pp. 1097–1100, July 1992.

[24] A. Rofougaran, J. Rael, M. Rofougaran, and A. Abidi, "A 900 mhz cmos lc-oscillator with quadrature outputs," in *1996 IEEE International Solid-State Circuits Conference. Digest of TEchnical Papers, ISSCC*, Feb 1996, pp. 392–393.

[25] Jae Joon Kim and Beomsup Kim, "A low-phase-noise cmos lc oscillator with a ring structure," in *2000 IEEE International Solid-State Circuits Conference. Digest of Technical Papers (Cat. No.00CH37056)*, Feb 2000, pp. 430–431.

[26] E. Norrman, "The inductance-capacitance oscillator as a frequency divider," *Proceedings of the IRE*, vol. 34, no. 10, pp. 799–803, Oct 1946.

[27] J. Lee and H. Wang, "Study of subharmonically injection-locked plls," *IEEE Journal of Solid-State Circuits*, vol. 44, no. 5, pp. 1539–1553, May 2009.

[28] B. Razavi, "A study of injection locking and pulling in oscillators," *IEEE Journal of Solid-State Circuits*, vol. 39, no. 9, pp. 1415–1424, Sep. 2004.

[29] C. Wang, Z. Chen, and P. Heydari, "W-band silicon-based frequency synthesizers using injection-locked and harmonic triplers," *IEEE Transactions on Microwave Theory and Techniques*, vol. 60, no. 5, pp. 1307–1320, May 2012.

[30] M. Chen and C. Wu, "Design and analysis of cmos subharmonic injection-locked frequency triplers," *IEEE Transactions on Microwave Theory and Techniques*, vol. 56, no. 8, pp. 1869–1878, Aug 2008.

[31] Z. Chen and P. Heydari, "An 85-95.2 ghz transformer-based injection-locked frequency tripler in 65nm cmos," in *2010 IEEE MTT-S International Microwave Symposium*, May 2010, pp. 776–779.

[32] S. Jang, C. Chang, C. Cheng, C. Hsue, and C. Hsu, "A wide-locking range sige bicmos divide-by-3 injection locked oscillators," in *Proceedings of 2011 International Symposium on VLSI Design, Automation and Test*, April 2011, pp. 1–4.

[33] C. Lee, W. Ma, and N. L. Wang, "Averaging and cancellation effect of high-order nonlinearity of a power amplifier," *IEEE Transactions on Circuits and Systems I: Regular Papers*, vol. 54, no. 12, pp. 2733–2740, Dec 2007.